# Impact of vehicular emissions on the formation of fine particles in the Sao Paulo Metropolitan Area: A numerical study with the WRF-Chem model

**Angel Vara-Vela[1], M. F. Andrade[1], Prashant Kumar[2,3], R. Y. Ynoue[1], and A. G. Muñoz[4,5]**

[1]Department of Atmospheric Sciences, Institute of Astronomy, Geophysics and Atmospheric Sciences, University of Sao Paulo, Sao Paulo, Brazil

[2]Department of Civil and Environmental Engineering, Faculty of Engineering and Physical Sciences (FEPS), University of Surrey, Guilford GU2 7XH, United Kingdom

[3]Environmental Flow (EnFlo) Research Centre, Faculty of Engineering and Physical Sciences, University of Surrey, Guildford GU2 7XH, United Kingdom

[4]International Research Institute for Climate and Society (IRI), The Earth Institute, Columbia University, NY, USA

[5]Centro de Modelado Científico (CMC), Universidad del Zulia, Maracaibo, Venezuela

Corresponding author: A. V. Vela (angel.vela@iag.usp.br)

## Abstract

The objective of this work is to evaluate the impact of vehicular emissions on the formation of fine particles ($PM_{2.5}$; ≤2.5 μm in diameter) in the Sao Paulo Metropolitan Area (SPMA) in Brazil, where ethanol is used intensively as a fuel in road vehicles. The Weather Research and Forecasting with Chemistry (WRF-Chem) model, which simulates feedbacks between meteorological variables and chemical species, is used as photochemical modelling tool to describe the physico-chemical processes leading to

evolution of number and mass size distribution of particles through gas-to-particle conversion. A vehicular emission model based on statistical information of vehicular activity is applied to simulate vehicular emissions over the studied area. The simulation has been performed for a one month period (7 August - 6 September 2012) to cover the availability of experimental data from the NUANCE-SPS (Narrowing the Uncertainties on Aerosol and Climate Changes in Sao Paulo State) project that aims to characterize emissions of atmospheric aerosols in the SPMA. The availability of experimental measurements of atmospheric aerosols and the application of the WRF-Chem model made it possible to represent some of the most important properties of fine particles in the SPMA such as the mass size distribution and chemical composition, besides allowing us to evaluate its formation potential through the gas-to-particle conversion processes. Results show that the emission of primary gases, mostly from vehicles, led to a production of secondary particles between 20 and 30 % in relation to the total mass concentration of $PM_{2.5}$ in the downtown SPMA. Each of $PM_{2.5}$ and primary natural aerosol (dust and sea salt) contributed with 40-50% of the total $PM_{10}$ (i.e. those $\leq$10 μm in diameter) concentration. Over 40% of the formation of fine particles, by mass, was due to the emission of hydrocarbons, mainly aromatics. Furthermore, an increase in the number of small particles impaired the ultraviolet radiation and induced a decrease in ozone formation. The ground level $O_3$ concentration decreased by about 2% when the aerosol-radiation feedback is taken into account.

## 1. Introduction

The Sao Paulo Metropolitan Area (SPMA), in the southeast region of Brazil, is considered a megalopolis comprised of Sao Paulo city and more 38 municipalities. One of the main concern in the SPMA is the occurrence of violations of air quality standards

for ozone and fine particles at different air quality stations from the Sao Paulo Environmental Agency (CETESB). The air pollutant emissions in the SPMA are related to the burning of the fuels: ethanol, gasohol (gasoline with 25% ethanol) and diesel. Recent work of Carvalho et al. (2014) reported a substantial increase in number of road vehicles from 1 million in 2000 to almost 7 million in 2014, together with an overview of the pollutants concentration, fuel use in the SPMA and the relationship between the emissions and the improvement in the air quality in past years.

They constitute the main cause of impairment to air quality in the SPMA, but the number of air quality standard violations has decreased for almost all pollutants with the exception of $PM_{2.5}$ and $O_3$. Both these pollutants are impacted by the vehicular emissions and have experienced an increase in the number of violations of local air quality standards as discussed in detail by Carvalho et al. (2014). Pérez-Martínez et al. (2015) have analyzed the monthly mean values for the regulated pollutants from 2000 to 2013 for the air quality stations in the SPMA. They found a decrease in the average concentration of NOx, CO and $PM_{10}$ by 0.65, 0.37 and 0.71 % $month^{-1}$, respectively, although the sales of the fuels (gasoline, ethanol, and diesel) had increased by 0.26, 1.96 and 0.38 % $month^{-1}$, respectively.

A recent report from CETESB (CETESB, 2013) highlighted that, in 2012, the vehicles contributed with about 40% of the total $PM_{10}$ mass concentrations through direct emissions. If we consider the secondary aerosols, which were about 25% of $PM_{10}$ as estimated by CETESB (2013), these were mainly found to be formed by chemical reactions between gases released from exhaust of vehicles.

The implementation of the Program for the Control of Vehicular Emission (PROCONVE) established by the Brazilian Government in the 80's, enforcing measures such as use of catalytic converters and ethanol as additive to gasoline in substitution of

tetraethyllead, led to decrease in emissions of CO and VOCs and hence their ambient concentration. Although the emissions have been controlled by regulations, the number of vehicles has increased substantially and faster than the replacement of the old vehicles by the new ones (Pérez-Martínez et al., 2014). According to CETESB (2013), the road vehicles contributed up to about 97, 87 and 80% of CO, VOCs and NOx emissions in 2012, respectively.

To date, many studies assessing the impact of biofuels on the air quality have been performed in Brazil. For example, Anderson (2009) conducted a review concerning the use of ethanol fuel in Brazil. His work highlighted that the atmospheric concentrations of acetaldehyde and ethanol are much higher in Brazil in comparison with the other areas of the world. Costa and Sodré (2010) showed that exhaust emissions of hydrous ethanol reduced CO and Hydrocarbons (HC), but increased $CO_2$ and NOx levels.

A number of past studies has shown the significant participation of the carbonaceous compounds in the concentration of fine particles in the SPMA (Albuquerque et al., 2011; Miranda and Andrade, 2005; Ynoue and Andrade, 2004; Castanho and Artaxo, 2001). Studies conducted on ambient air pollution in the SPMA have also shown that black carbon (BC) explains 21% of mass concentrations of fine particles ($PM_{2.5}$; ≤2.5 μm in diameter) compared with 40% of organic carbon (OC), 20% of sulfates, and 12% of soil dust (Andrade et al., 2012). Most of the observed ambient $PM_{2.5}$ mass concentration usually originates from precursors gases such as sulphur dioxide ($SO_2$), ammonia ($NH_3$), nitrogen oxides (NOx) and volatile organic compounds (VOCs) as well as through the physico-chemical processes such as the oxidation of low volatile hydrocarbons noted above transferring to the condensed phase (McMurry et al., 2004; Heal et al., 2012). Since these processes are often photo-

chemically driven, the resultant aerosol usually falls into the category of secondary photochemical pollutant (Jenkin and Clemitshaw, 2000). Oxidation of VOCs can produce species of sufficiently low vapor pressure to be condensable, leading to the formation of secondary organic aerosol (SOA) (Kroll and Seinfeld, 2008). Fine particles in SPMA have a great participation on its composition of SOA, formed from the emissions of VOCs, which have the same origin of the primary compounds involved in the formation of ozone, from the burning of fuels. The participation of the biogenic emission is considered to be small in the formation of particles in the metropolitan area of the city according to previous studies of Martins et al. (2006).

The impact of the fine particles has been discussed in previous works, with evaluation of the scattering and absorbing effects of the aerosol (e.g. Li et al., 2005; Real et al., 2011). Vehicular emissions of particulate matter (PM) in the SPMA have a high percentage of BC (Brito et al., 2013), which after emitted to the atmosphere can enhance the absorption coefficient and thus the attenuation rates.

One of the most important aspects of this work is the quantitative analysis of the formation of $PM_{2.5}$ and ozone ($O_3$) in the SPMA. Photolysis of $O_3$ by ultraviolet light in the presence of water vapor is the main source of hydroxyl radical (OH), the most important radical in the atmosphere in terms of reactivity (Monks, 2004). At the same time, OH levels in the atmosphere directly determine the oxidation rate of the precursors of secondary aerosols. Oxidation products of VOCs and semi-VOCs by OH are the most important precursors of SOA (Li et al., 2011a). Although VOCs and NOx are precursors of both $O_3$ and a fraction of atmospheric PM ($NO_3^-$ and secondary organics) while they influence indirectly the formation of the rest of the secondary PM components like $SO_4^=$, their control strategies that are optimal for $O_3$ controls may even increase $PM_{2.5}$ concentrations (McMurry et al., 2004). Such an analysis is important to

evaluate the contribution of the vehicular fleet using different kind of fuels to the concentration of fine particles. In this sense, a numerical study with an adequate physical approach, representing particles in the modelling system, is important to understand the formation of secondary aerosols from primary emission of gases in a metropolitan area where the composition of fuel in vehicular fleet has changed significantly over the past years. Therefore, the goal of the present study is to evaluate the impact of vehicular emissions on the formation of fine particles in the SPMA, focusing especially on the potential formation of secondary particles from the primary emission of gases coming from on-road vehicles. The impact of aerosol particles on the ozone photochemistry is also examined by means of numerical simulations. Measurements were performed to provide input data to evaluate the modelling performance and estimate the vehicular emission factors. Aerosol measurements were taken from field campaigns that were carried out as part of the Narrowing the Uncertainties on Aerosol and Climate Changes in Sao Paulo State (NUANCE-SPS) project (http://nuance-lapat.iag.usp.br/). These campaigns took place between July and September 2012. An online-coupled meteorology and chemistry model, i.e., the Weather Research and Forecasting with Chemistry (WRF-Chem) model, has been used to characterize and describe the physico-chemical processes involved in both the formation and growth of new particles over the SPMA in southern Brazil. The details of the experimental campaigns, WRF-Chem model and emissions are described in Section 2. Results from modelling experiments and comparison with measurements are presented in Section 3. Finally, the summary and conclusions are given in Section 4.

## 2. Methodology

### 2.1. Observational datasets

151 The study period starting from 7 August until 6 September 2012 was selected for
152 comparison with the modelled results (Section 2.2) due to the availability of
153 experimental data from the NUANCE-SPS project. The aim of NUANCE-SPS was to
154 evaluate the impact of emissions in the SPMA on the air quality and changing climatic
155 conditions, and feedback mechanisms between climatic perturbations produced by both
156 primary and secondary emissions and urban atmospheric processes. Aerosol observation
157 datasets used in this work were collected using a Dichotomous sampler (Wedding et al.,
158 1980) and a Micro-Orifice Uniform Deposit Impactor (MOUDI, model 100; MSP
159 Corporation - Marple et al., 1986). The MOUDI impactor collected particles in 10 size
160 classes with nominal 50% cut-off diameters: 10, 5.6, 3.2, 1.8, 1.0, 0.56, 0.32, 0.18, 0.1
161 and 0.06 μm. Particles smaller than 0.06 μm were collected in a subsequent stage or
162 after-filter. The samples collected with the MOUDI impactor were deposited on a
163 polycarbonate membrane filter with 0.4 μm porous and for the Dichotomous sampler
164 the substrate was a teflon membrane filter with 2 μm porous. The after-filter in the
165 MOUDI impactor is a 33 mm teflon membrane filter, which was not submitted to the
166 reflectance analysis. The collected membrane filters sampled with the Dichotomous and
167 MOUDI samplers were analyzed to the identification of trace elements of mass through
168 X-ray diffraction analysis, mass concentration through gravimetric analysis, and black
169 and organic carbon through reflectance and thermo analysis using a thermal-optical
170 transmittance (TOT) (Sunset Laboratory Inc. – Birch and Cary, 1996). Ion
171 concentrations were evaluated through the ion chromatography analysis of the soluble
172 material collected on the membrane filters (sulphate, nitrate, ammonium, sodium, and
173 chloride). All these samplings were performed on the roof of the main building of the
174 Institute of Astronomy, Geophysics and Atmospheric Sciences of the University of Sao
175 Paulo (IAG-USP) (hereafter also referred as IAG-USP measurement site or simply

IAG-USP), which is inside a small green-park (approximately 7.4 $km^2$), with local traffic during the day and surrounded by major roads with intense traffic by light and heavy-duty vehicles (Nogueira et al., 2014). Table 1 lists the aerosol instrumentation deployed roughly at the IAG-USP measurement site. In addition, ambient data from the CETESB's air quality monitoring network and the IAG-USP's climatological station (hereafter also referred as AF-IAG) were also considered for evaluation of numerical simulations. The locations of measurement sites are depicted in Fig. 1 whereas geographic coordinates and the list of pollutants and meteorological parameters monitored at each site is available in Table 2.

## 2.2. WRF-Chem model

The WRF-Chem model is a fully coupled online meteorological and chemical transport model (Grell et al., 2005), supported by National Center for Atmospheric Research (NCAR) of the USA and several other research institutions around the world. This model is a system of two key components. The WRF-Chem meteorological component, the Weather Research and Forecasting (WRF), is a system configured for both research and operational applications. The dynamical core used in this study is the Advanced Research WRF (ARW). Model's equations into ARW are solved to non-hydrostatic conditions on a fully compressible atmosphere. Further details on the modelling system can be found on the WRF model website (http://www.wrf-model.org). On the other hand, the WRF-Chem chemical component treats chemical processes such as dry deposition, gas-phase chemistry, photolysis rates, and aerosols chemistry. A detailed description of the WRF-Chem model can be found on its website (http://ruc.noaa.gov/wrf/WG11). Since both meteorological and chemical components are fully coupled, the transport of all chemical species is on-line. The gas-phase

chemistry and aerosol modules employed in this study are the Regional Acid Deposition Model, version 2 (RADM2) (Chang et al., 1989) and the Modal Aerosol Dynamics Model for Europe - Secondary Organic Aerosol Model (MADE - SORGAM) (Ackermann et al., 1998; Schell et al., 2001), respectively. The inorganic species included in the RADM2 mechanism are 14 stable species, 4 reactive intermediates, and 3 abundant stable species (oxygen, nitrogen and water). Atmospheric organic chemistry is represented by 26 stable species and 16 peroxy radicals. The RADM2 mechanism represents organic chemistry through a reactivity aggregated molecular approach (Middleton et al., 1990). Similar organic compounds are grouped together in a limited number of model groups through the use of reactivity weighting. The aggregation factors for the most emitted VOCs are given in Middleton et al. (1990).

On the other hand, the most important process for the formation of secondary aerosol particles is the homogeneous nucleation in the sulfuric acid-water system. It is parameterized in MADE, following the method of Kulmala et al. (1998). Aerosol growth by condensation occurs in two steps: the production of condensable material (vapor) by the reaction of chemical precursors, and the condensation and evaporation of ambient volatile species on aerosols. The inorganic chemistry system, based on the Model for an Aerosol Reacting System (MARS) (Saxena et al., 1986) and its modifications by Binkowski and Shankar (1995), calculates the chemical composition of a sulphate-nitrate-ammonium-water aerosol according to equilibrium thermodynamics. The organic aerosol chemistry is based on the SORGAM, which assumes that SOA compounds interact and form a quasi-ideal solution (Grell et al., 2005). The SOA formation in SORGAM follows the two-product approach (Odum et al., 1996) where the oxidation of hydrocarbons produces two types of modelled semivolatile compounds that are partitioned between the gas and particle phases after

considering the absorptive partitioning theory (Pankow, 1994a; b). The primary organic aerosol (POA) in MADE is calculated from the primary anthropogenic emission of OC. Then, one may calculate the predicted OC concentration from the sum of both SOA and POA. The concurrent organic matter (OM) can be obtained from the OC concentration by application of a conversion factor. Brown et al. (2013) showed that the average OM:OC ratio was 1.54 (with a standard deviation of 0.2) for sites with low amount of secondary aerosol formation. It is important to note that this ratio can change from one place to another. In areas impacted by biomass burning the ratio can be higher. Gorin et al. (2006) assumed a ratio of 1.6 for the conversion from OC to OM over an area that experiences a significant wood smoke influence.

### 2.2.1. Model configuration

WRF-Chem version 3.5 was configured with three nested grid cells: coarse (75 km), intermediate (15 km) and fine (3 km). The coarse grid cell covered a big region of Brazil and also of the Atlantic Ocean. The intermediate grid covered the southeast Brazil while the fine grid cell covered barely the SPMA and metropolitan areas nearest to it. Fig. 1 shows the arrangement of measurement sites and topography in the downtown area of the 3-km modelling domain. The initial and boundary meteorological conditions are from the National Center for Environmental Prediction's Final Operational Global Analysis with $1^{o}$ of grid spacing, 26 vertical levels and are available every six hours: 00, 06, 12 and 18 UTC (http://rda.ucar.edu/datasets/ds083.2/). The initial and boundary chemical conditions for representing gases and aerosols background concentration were obtained from the Model for Ozone and Related chemical Tracers, version 4 (MOZART-4; Emmons et al., 2010). This model was driven by meteorological inputs from the Goddard Earth Observing System Model,

version 5 at a horizontal resolution of $1.9^{o}\times2.5^{o}$, 56 vertical levels that are also available every six hours. Table 3 lists the WRF-Chem configuration options employed by this study.

WRF-Chem simulation with coupled primary aerosol (dust, sea salt and anthropogenic) and gas (biogenic and anthropogenic) emission modules, together with the direct effect of aerosol particles turned on, is performed as the control simulation in order to evaluate the model performance (hereafter referred to as Case_0). For secondary aerosols, a simulation scenario (Case_1) with biogenic and anthropogenic gases emission is performed to evaluate its formation potential. An additional simulation (Case_2) is also performed to evaluate the impact of aerosols on ozone photochemistry. Notation and description of simulations are listed in Table 4. The first seven days of each simulation were not analyzed and used for model spin-up.

## 2.3. Emissions

### 2.3.1. Anthropogenic emissions

Anthropogenic emissions of trace gases and particles in both 3 and 15 km modelling domains were considered to include emissions only coming from on-road vehicles through the use of a vehicular emission model developed by the IAG-USP's Laboratory of Atmospheric Processes (LAPAt). Basically, this model considers the number of vehicles, vehicular emission factors, and average driving kilometers for vehicle per day as basic parameters for the calculation of exhaust emissions considering different vehicle types (light-duty vehicles, heavy-duty vehicles, and motorcycles) and different fuel types (ethanol, gasohol, combination of any proportion of gasohol and ethanol, and diesel) according to CETESB (2012). The details of this model are available in Andrade et al. (2015). In the case of VOCs, there are other two relevant

276 emissions (fuel transfer and evaporative processes) associated with the vehicles, besides
277 the exhaust emissions. Because of the complexities in the spatial representation due to a
278 numerous factors such as emissions at service stations, such emission sources are
279 assumed to be emitted by exhaust of vehicles for the sake of simplicity. The vehicular
280 fleet and intensity of use datasets are provided by the National Department of Traffic
281 (DENATRAN) and the Sao Paulo Transporte (SPTrans), respectively. Emission factors
282 for road vehicles for most pollutants were considered from previous studies performed
283 inside the road tunnels (i.e. Janio Quadros, referred as JQ tunnel, and the tunnel 3 of the
284 Rodoanel Mario Covas that is referred hereafter as RA tunnel) located within the SPMA
285 (Pérez-Martínez et al., 2014; Nogueira et al., 2014). However, emission factors for
286 VOCs are considered from dynamometer protocols (CETESB, 2010). VOCs and
287 particulate matter speciation profiles used by pas-phase and aerosol chemical modules
288 were also obtained from NUANCE-SPS experimental campaigns performed in 2011
289 (tunnel measurements) and 2012 (ambient data). It is important to note that due to the
290 lack of information on vehicular emission factors and intensity of use for most of the
291 other metropolitan areas inside both modelling domains (e.g. the Campinas
292 Metropolitan Area, which is shown by the second largest grey stain in Fig. 2), the
293 calculation of vehicular emissions for these urban areas was carried out on the basis of
294 the parameters found for the SPMA. The number of vehicles in any modelling domain
295 is calculated from the sum of the number of vehicles in each one of the main urban
296 areas inside the modelling domain in question.

297 Spatial distribution of emissions for the 3 km modelling domain resolution was
298 based on road density products compiled by the OpenStreetMap project and extracted
299 from the Geofabrik's free download server (http://download.geofabrik.de). Urban areas
300 were assumed to allocate high emissions since these concentrate a road density greater

than other areas. In the case of the 15 km modelling domain, emissions are based on night-time lights data from the Defense Meteorological Satellite Program (http://ngdc.noaa.gov/eog/dmsp/downloadV4composites.html). These images are 30 arc second grids, spanning from -180$^{o}$ to +180$^{o}$ longitude and -65$^{o}$ to +75$^{o}$ latitude and contain the lights from cities, towns and other sites with persistent lighting, including gas flares. Cleaned up night-time light points with no ephemeral events such as forest fires are used to allocate emissions. To estimate the number of vehicles in each grid point of both domains, the sum of individual intensities at each point (i.e. total road length for the 3 km modelling domain and night-time light for the 15 km modelling domain) is firstly normalized by the total fleet, and then distributed uniformly using the total fleet distribution so that emissions in urban areas are mainly represented by emissions coming from their vehicles. Furthermore, due to the complexity involved in describing the temporal variation of emissions at each grid point, median values for vehicular traffic obtained from measurements inside the JQ and RA tunnels (Pérez-Martínez et al., 2014) were used for distributing the emissions during the day in both domains. This approximation followed the approach used by Fast et al. (2006) where emission profiles were calculated from median diurnal variations on weekdays and weekends. We have applied the same constant diurnal cycle at all grid points where emissions have values greater than zero. VOC and PM emission profiles were assumed to be the same as for CO and NOx emission profiles since these pollutants are also characteristic tracers of emissions of light-duty and heavy-duty vehicles, respectively. Fig. 2 shows the maximum hourly emission rates for aromatic VOCs in the 3 km modelling domain. Anthropogenic emissions were not considered in the 75 km modelling domain.

The Another Assimilation System for WRF-Chem (AAS4WRF) chemical emissions pre-processor developed by the Latin American Observatory (OLE2; Muñoz et al., 2010; 2012) was used to scale emission rates on WRF curvilinear coordinates. AAS4WRF is appropriate to write chemical emission rates from both surface and elevated sources in the proper WRF data file format, providing an alternative tailored way to assimilate emissions to WRF-Chem. The method is explained in the OLE2 Wiki pages in detail (http://www.cmc.org.ve/mediawiki/index.php?title=Calidad_de_Aire).

### 2.3.2. Other emissions

Biogenic emissions are calculated online based on the Guenther scheme (Guenther et al., 1993; 1994). The Guenther biogenic emissions model calculates the emission rates using temperature, photo-synthetically active radiation flux and land-use data as the U.S. Geological Survey (USGS) land-use cover system classification if coupled with the WRF model. However, as indicated in the WRF-Chem emissions guide (http://ruc.noaa.gov/wrf/WG11/Emission_guide.pdf), several key chemical species would have been representing relatively low emission rates because of the limited vegetation types in the simulation, and thus their impacts are anticipated to be much lower than those from vehicular emissions.

Dust and sea salt emissions are calculated online following the works of Ginoux et al. (2001) and Gong (2003), respectively. The calculation of Ginoux et al. (2001) for the uplifting of dust particles is based on the surface wind speed, wetness and information on soil characteristics. The model then solves the continuity equation including the emission, chemistry, advection, convection, diffusion, dry deposition, and wet deposition of each species. The parameterization of sea salt aerosol source function of Gong (2003) is an extended parameterization of Monahan et al. (1986), which scales

the generation of marine aerosols from mechanical disruption of wave crests by the wind and sea surface covered by whitecaps.

## 3. Results and discussion

### 3.1. Characterization of meteorological conditions

In order to study and understand the spatial and temporal variability of atmospheric aerosols, $O_3$, and other pollutants (i.e. CO, NOx) during the study period, it was first necessary to analyze the behavior of main meteorological systems acting on the atmospheric environment of the SPMA and surrounding areas.

According to the monthly climate reports from the IAG-USP's Climate Research Group (GrEC), the observed precipitation rates were lower than the climatological value in SPMA (anomaly of -38.6 mm) and larger part of the Sao Paulo State during August 2012. Negative anomalies on the precipitation were caused by the intensification of the South Atlantic Subtropical High (SASH). These conditions established an easterly wind anomaly pattern at the 850 hPa level. Conditions were unfavorable for relative humidity coming from the Amazon due to the Low Level Jet (LLJ) and less intense Alisian winds in the Tropical Atlantic (GrEC, 2012a). However, the action of frontal systems favored the rain accumulation in September 2012, mainly in western Sao Paulo State where the greater positive amount of anomalies was observed. Precipitation events were predominantly observed during the second half of the month. In this case, the wind pattern showed an opposite configuration to that observed in August 2012 as a result of the weakening of the SASH (GrEC, 2012b). The IAG-USP's climatological station recorded an accumulated precipitation of about 1.3 mm on three days of occurrence (28 August, 30 August and 4 September 2012) and an easterly wind pattern with a median intensity of 2 m $s^{-1}$ during the period between 07 August and 06 September 2012. Fig. 3

shows the hourly accumulated precipitation and relative humidity observed at the IAG-USP's climatological station.

### 3.2. Analysis of aerosol species

Aerosol analysis included species such as organic carbon (OC), elemental carbon (EC), sulphate, nitrate, ammonium, sodium and chloride in addition to other elemental constituent of PM. All the sampling for these species were performed at IAG-USP. Results showed that the major contributors to the concentration of fine particles are OM (55.7%; OM:OC ratio of 1.5 found by Brito et al. (2013)) and EC (15%), followed by sulphate (2.9%), ammonium (2.1%), sodium (1.9%), nitrate (0.5%) and chloride (0.3%). The remaining mass (21.6%) is calculated by determining of the difference between the total mass of $PM_{2.5}$ (from the gravimetric analysis) and the sum of the masses of 7 individual compounds, as noted above. Part of this remaining mass is related to the water content of aerosols (Andrade et al., 2012).

On the other hand, $PM_{2.5}$, $PM_{10}$ and size distribution of particles measured at IAG-USP show that the study period was characterized by a reduction in the concentrations up to the end of August 2012 when their minimum values were achieved. This reduction was related to the action of a semi-stationary front between the coasts of Sao Paulo and Parana States. After the passage of this system, aerosol concentrations have significantly increased what could be related to an increase in relative humidity once the SASH system is moved away from the continent, as well as the transport of aerosol particles produced by forest fires in the central-west region of Brazil and the Sao Paulo State. Several studies have shown the contribution of forest

fires on the atmospheric aerosol concentrations in SPMA (Vieira-Filho et al., 2013; Vasconcellos et al., 2010). One way to qualitatively evaluate the contribution of forest fires on aerosol concentrations is by using the air mass trajectories. The Hybrid Single-Particle Lagrangian Integrated Trajectory (HYSPLIT) model (Draxler and Hess, 1998) was used to calculate backward trajectories of air masses in order to identify atmospheric transport of air mass from forest fire areas. Fig. 4 shows the three-day backward trajectories of air masses starting at IAG-USP for the days 9 and 31 August and 5 September, when increases in the OC and EC concentrations were observed at IAG-USP. The pink markers on the map represent the observed fire locations during the study period considering different satellite products (GOES, AQUA, TERRA, NOAA).

Fig. 5 shows the concentration of OC, EC and some species of $PM_{2.5}$ during the study period at IAG-USP. We can observe eleven exceedances of $PM_{2.5}$ concentration with respect to the air quality standard of 25 μg $m^{-3}$ (see grey line in Fig. 5a) established by the World Health Organization (WHO). These exceedances have mainly occurred at the beginning and at the end of the study period when an increase in the concentrations of OC and EC were observed. The increasing organic matter could be associated to traffic incidents which may raise the emissions, which in case of less favorable meteorological conditions (e.g. lower height of lower planetary boundary layer, PBL, or slow transport of air pollutants) may have led to a more efficient formation of secondary particles. Castanho and Artaxo (2001) analyzed the behavior of the aerosol composition in SPMA and showed the increase in the concentration of inorganic and organic material in the winter season compared to the summer season, explaining this behavior with the meteorological characteristics: dry conditions with low height inversion layer in the wintertime and a rainy summer.

Size distributions of aerosol mass indicate that the majority of sulphate, ammonium and $PM_{10}$ mass concentration is distributed in the size range with diameters between 0.1 and 1 µm, commonly known as accumulation mode particles (Kumar et al., 2010). In the cases of nitrate, sodium, and chloride, most part of mass was concentrated in particles with diameters greater than 1 µm.

### 3.3. Comparison of baseline simulation with observations

All the numerical results presented in this section, for the purpose of comparison with the measurements, were obtained from the baseline simulation (Case_0). The predicted temperature, humidity, and wind distribution have been compared to measurements from the AF-IAG and INT measurement sites. Overall, the model captured the diurnal variation of temperature, humidity, and wind directions reasonably well. However, the predicted wind speeds were slightly lower than the observed values. To evaluate the model performance in solving the meteorology and chemical species, we computed the statistics correlation coefficient (R), Bias (B), and root mean square error ($RMSE_{UB}$). The definitions of these statistics are given in the Appendix. Table 5 presents the summary of these statistics, showing comparisons between WRF-Chem predictions and observations. Fig. 6 shows the predicted average of wind vectors at 10 m and temperature at 2 m for the whole study period in the 3 km modelling domain. Blue dots represent the locations of AF-IAG and INT sites, while the numbers in cyan indicate the observed average temperatures (i.e. 17.7 °C at AF-IAG and 17.8 °C at INT). On an average, the predicted wind direction was easterly in SPMA, which has somewhat affected the spatial distribution of aerosol particles as examined later in this section. Likewise, a good agreement is found between the predicted $PM_{2.5}$, $PM_{10}$ and $O_3$ concentration and measurements at most of the sites. Figs. 7, 8 and 9 show the observed

447 and predicted temporal variations of $PM_{2.5}$, $PM_{10}$ and $O_3$ concentrations at 3, 10 and 6
448 sites in the SPMA, respectively, with some measurement sites sharing the same grid
449 point for comparisons due to the geographical proximity. These figures suggest that
450 predicted concentrations did not present any significant spatial variation in the
451 downtown SPMA and were generally underestimated when compared to measurements.
452 This under prediction could be associated with an underestimation on the vehicular
453 emissions as well as other emission sources (e.g. emissions coming from industry) that
454 are disregarded in this study, in addition to predicted surface winds more intense than
455 those observed, leading to a dilution of aerosol particles in SPMA. The high
456 concentrations of $PM_{2.5}$ and $PM_{10}$ observed at the beginning and at the end of the study
457 period, whose variability and trends were reasonably well captured by the model, could
458 be related with the emission of high aerosol loadings due to traffic incidents as well as
459 the establishment of lower PBL heights, commonly observed under post-frontal
460 situations. The results for this simulation (Case_0) show that overall the predicted PBL
461 heights (not shown here) have a regular diurnal variation in the downtown SPMA with
462 averaged daily values around 500 m at both the beginning and the end, and of up to 700
463 m in the middle of the study period, when lower concentrations of aerosols were
464 observed. Statistics to quantify the model performance in the representation of $PM_{2.5}$,
465 $PM_{10}$ and $O_3$ concentrations can be visualized along with the Taylor Diagram (Taylor,
466 2001) shown in Fig. 10. In general, most of evaluated parameters present good
467 correlation coefficients, mainly those for $PM_{10}$, but with negative biases and standard
468 deviations lower than those for observations. The mean biases for $PM_{2.5}$, $PM_{10}$ and $O_3$
469 concentrations were -8.84 $\mu g\ m^{-3}$, -14.13 $\mu g\ m^{-3}$ and -0.85 ppb, respectively (see Table
470 5).

Figures 11-13 show the predicted average surface distribution of $PM_{2.5}$, $PM_{10}$ and $PM_{2.5}$:$PM_{10}$ ratio for the 3 km modelling domain, respectively. Red dots and cyan numbers represent the locations and the observed mean PM concentrations (or mean PM concentration ratios) at the measurement sites, respectively. Major contributions of $PM_{2.5}$ on the total $PM_{10}$ concentration were observed mainly over offshore continental areas (see Fig. 13). High $PM_{2.5}$:$PM_{10}$ concentration ratios would be firstly associated with the transportation of fine particles and gases from upwind regions (see Fig. 6), followed by a production of fine particles from biogenic emissions. Additional comparisons between the observed and predicted concentrations of OC and EC at IAG-USP (the only site with measurements of OC and EC) are shown in Fig. 14. In addition to an underestimation of emissions, under predicted OC concentrations could also be associated with an underestimation of SOA probably due to the absence of oxidation of monoterpenes and a limited treatment of anthropogenic VOCs oxidation in the RADM2 mechanism, as discussed by Tuccella et al. (2012). The SORGAM aerosol module considers the formation of anthropogenic SOAs from the oxidation of alkane, alkene and aromatic VOCs as well as the biogenic SOA formation from the oxidation of alpha-pinene, limonene and isoprene VOCs. Recent studies coupling non-traditional SOA models (volatility basis set approaches) in WRF-Chem show improvements in the predicted SOA concentrations, although these are still lower than those observed (e.g. Li et al., 2011b; Ahmadov et al., 2012; Shrivastava et al., 2013).

On the other hand, measurements of mass size distribution were also made with a MOUDI impactor at IAG-USP, following the protocol describe in Miranda and Andrade (2005). Constituents of aerosol were subsequently determined by X-Ray fluorescence analysis and ion chromatography analysis. As previously indicated in this section, the main identified species are $SO_4$, $NO_3$, $NH_4$, Na and Cl. The observed

496 average aerosol composition is derived using measurements from both MOUDI
497 impactor and SUNSET analyzer. To perform the comparisons of mass size distribution,
498 we adequately joined the MOUDI bin sizes according to the three modes used by the
499 MADE aerosol module: Aitken (<0.1 μm), accumulation (0.1-1 μm) and coarse (>1
500 μm). The observed and predicted aerosol mass size distributions averaged over the same
501 sampling time period (16 days along the study period) are shown in Fig. 15. Over the
502 downtown SPMA, both the observed and predicted fine particles from accumulation
503 mode account for majority of the total $PM_{2.5}$ mass. Since the formation-growth
504 processes of aerosols in question are explicitly treated in the Aitken and accumulation
505 modes, the predicted concentrations for particles larger than 1 μm are assumed to be
506 zero. In this case, the mass of particles larger than 1 μm is allocated to the $PM_{10}$ aerosol
507 variable (see Fig. 15). The comparison between the observed and predicted average
508 contributions for the main identified aerosol constituents at IAG-USP is shown in Fig.
509 16. Both the observed and predicted OC and EC make up the largest fraction of $PM_{2.5}$
510 mass with contributions of 55 and 40%, respectively. In addition, it was found that the
511 predicted SOA concentrations contribute 17% of the predicted total OC concentration at
512 this measurement site. Various global and regional scale SOA simulations have been
513 conducted using mass-based yield and partitioning coefficients, but they have
514 underestimated the SOA concentrations by roughly an order of magnitude, especially
515 over urban regions (Matsui et al., 2014). Using the same SOA formation approach
516 employed by this study and a conversion factor of 1.6 to convert the emissions of OC to
517 OM, Tuccella et al. (2012) found simulated SOA:OM ratios in the 5-40% range against
518 the observed range of 50-80%. Although the predicted average $PM_{2.5}$ concentration
519 (14.48 μg $m^{-3}$) was lower than observed (22.32 μg $m^{-3}$), the mean aerosol chemical
520 composition was reasonably well represented by the model (see Fig. 16).

### 3.4. Contribution of dust-sea salt and coarse anthropogenic aerosols to PM concentration

The evaluation of the contribution of dust and sea salt aerosols on $PM_{10}$ concentration is performed from the sum of their concentrations divided by the $PM_{10}$ concentration. The simulated average ratio between dust–sea salt aerosols and the total $PM_{10}$ mass concentration is shown in Fig. 17b. High concentration ratios have been observed over the ocean where sea salt emissions are by far the most important aerosols source. Unlike high concentration ratios over the ocean, lower concentration ratios are observed over the continent far away from the coast. In this region, the main sources of atmospheric aerosols would be the emission of primary biological aerosol, SOA formed from the emission of biogenic volatile organic compounds (BVOCs), and forest fires. However, particles could also be transported from remote areas. In addition, we can also observe that dust and sea salt aerosols have a contribution between 40 and 50% of the total $PM_{10}$ concentration in the downtown SPMA. Furthermore, it is possible to estimate the contribution of all the other $PM_{10}$ (i.e., the coarse anthropogenic aerosol) to the total $PM_{10}$ mass concentration. It may be directly calculated from the model or estimated from the Figs. 13 and 17b once the sum of concentrations of $PM_{2.5}$, dust and sea salt, and coarse anthropogenic aerosol represents 100% of the total $PM_{10}$ mass concentration. For example, we found that the coarse anthropogenic aerosol represents around 10% of $PM_{10}$ in the downtown SPMA.

### 3.5. Evaluation of secondary aerosol formation

As described in Section 2.1, aerosol module employed by this study (MADE/SORGAM) includes the homogeneous nucleation in the sulphuric acid-water system. The sulphuric acid is the most significant condensable molecule formed in the atmosphere, which has also been long recognised as the most important molecule from

546 the point of view of the nucleation of new particles (Jenkin and Clemitshaw, 2000;
547 Seinfeld and Pandis, 2006). However, for the SPMA, the importance of SOA formed
548 from the anthropogenic emission of fuel used by the transport sector was noted (Salvo
549 and Geiger, 2014). According to the official emission inventory developed by the Sao
550 Paulo Environmental Protection Agency (CETESB, 2013), the SOA explains 51% of
551 the fine particle mass concentration, with the vehicular emission being its main source.
552 The subsequent growth processes involve aerosol growth by condensation of
553 condensable material onto existing particles, and by coagulation of particles to form
554 larger particles (Kumar et al., 2011; 2014). For example, particles in the accumulation
555 mode emerge through coagulation of particles from the Aitken mode (Kumar et al.,
556 2011). It is important to emphasize that the boundaries were updated with gas and
557 aerosol background concentrations coming from the 15 km modelling domain during
558 the whole simulation period. Thereafter, the impact of vehicular emissions on the
559 formation of fine particles was calculated from the predicted $PM_{2.5}$ concentration
560 considering an emission scenario (Case_1) in which only emission of gases from
561 vehicles and vegetation are taken into account to be emitted to the atmosphere from the
562 surface. The predicted average $PM_{2.5}$ (Case_1):$PM_{2.5}$ (Case_0) ratio is shown in Fig.
563 17a. A contribution between 20 and 30% in the predicted baseline $PM_{2.5}$ concentration
564 in downtown SPMA is found to correspond to the fine particles formation and
565 transportation processes. Higher concentration ratios over the SPMA surroundings (30-
566 50%) could be associated with more efficient biogenic emissions. Overall, it is observed
567 that the formation efficiency increases towards the northwest from the ocean. Deep red
568 areas in Fig. 17a could also be associated with the transportation of fine particles and
569 gases from other regions, in addition to having a more efficient production of fine
570 particles from biogenic emissions. For example, given the distribution of winds in Fig.

6, the northern boundary could represent the main source of particles and gases over this part of the simulation domain. Additionally, the comparison between the predicted and observed OC and EC concentrations at IAG-USP shown in Fig. 14 includes the Case_1 simulation in which only emission of primary gases is taken into account in the assessment of fine particles formation. The concentration peaks observed at the beginning and at the end of the study period may be associated with the transport of aerosol particles from both biomass and fossil fuel burning areas (see Fig. 4). Considering the Case_1 simulation, we can observe very low concentrations for EC (mean concentration of 0.01 μg $m^{-3}$), as expected. This is because these particles are not produced by photochemical processes in the atmosphere, but associated mainly with the diesel exhaust.

### 3.6. Aerosol impact on $O_3$ photochemistry

Ozone photochemistry production mainly depends on the two key photolysis rates, as shown in Eqs. (1) and (2), i.e., shortwave radiation able to reach the surface to break molecules of $O_3$ and $NO_2$.

$$O3 + hv \rightarrow O2 + O(^1D)\ (\lambda < 320\ nm) \quad (1)$$

$$NO_2 + hv \rightarrow NO + O(^3P)\ (\lambda < 420\ nm) \quad (2)$$

Therefore, the impact of aerosols on $O_3$ photochemistry has been evaluated from the impact of aerosols on downward shortwave radiation. Attenuation (scattering and absorption) of downward shortwave radiation by aerosols may substantially modify the photolysis rates, and thereby affecting the ozone photochemistry production.

The average percentage change in surface $O_3$ concentrations at 16:00 h (local time) with and without the aerosol-radiation feedback module turned on are shown Fig.

17c. Overall $O_3$ is destroyed or formed (incoming transport from other regions) in small quantities between -1 and +1% in relation to its total concentration. In addition, it was observed that the surface $O_3$ concentration decreased by around 2% in the downtown SPMA. Li et al. (2011a) found that the impact of aerosols on $O_3$ formation in Mexico City was most pronounced in the morning with the $O_3$ reduction of 5-20%, but the reduction is less than 5% in the afternoon. Low reductions in the $O_3$ concentration in the downtown SPMA compared to results from other studies may be explained by the lower predicted $PM_{10}$ concentrations, which can lead to a minor attenuation of the incoming solar radiation. Simulated mean downward shortwave fluxes at ground surface (not shown) were up to 5% higher for the Case_2 than for the Case_0 during the afternoon. The inclusion of the direct effect of aerosol particles was found to have small reductions in the surface temperature (changes by around 2%), presumably due to an increase in the number of atmospheric processes involving downward longwave fluxes over this area. Forkel et al. (2012) found an underestimation of predicted downward longwave radiation over the southern Baltic Sea when the direct effect of aerosol particles was neglected. Despite the highly non-linear behavior of tropospheric $O_3$, the reduction in the predicted $O_3$ concentrations indicates a high efficiency of aerosols to attenuate the downward shortwave radiation, what is plausible once it was found that low $PM_{10}$ concentrations have a capability to reduce ground level $O_3$ concentrations in a few ppb.

## 4. Summary and conclusions

The WRF-Chem community model has been used to evaluate the impact of vehicular emissions on the fine particles formation in the SPMA. Three thirty-one day simulations, covering a period from 7 August to 6 September 2012, have been performed. The aims were to evaluate the impact of fine particles formation (both inorganic and SOA) from gases emitted by road vehicles as well as the aerosol impacts

on the ozone formation photochemistry. The results were compared with the measurements available from the NUANCE-SPS project.

The predicted temporal variations of meteorology, $PM_{2.5}$, $PM_{10}$ and $O_3$ were found to agree well with the measurements at most of the sites during the entire simulation period. However, the predicted concentrations of $PM_{2.5}$, $PM_{10}$ and $O_3$ (but in minor intensity) were lower than the observed values. This difference could be associated with an underestimation of the vehicular emissions and other emission sources such as industry, heating and cooking, which are not considered in this study. Wind speed and direction played an important role in the distribution of fine particles over the simulation domain. Backward trajectories analysis suggested that aerosol particles from biomass burning were transported to SPMA, impacting on the PM concentration over this region.

The baseline simulation (Case_0) showed that dust and sea salt aerosols made a contribution between 40 and 50% of the total $PM_{10}$ concentration in the downtown SPMA. On the other hand, the Case_1, which represents simulations with gaseous emissions only, indicates that the emissions of primary gases coming mainly from vehicles have a potential to form new particles between 20 and 30% in relation to the baseline $PM_{2.5}$ concentration found in the downtown SPMA. Finally, the Case_2, which represents simulations with aerosol-radiation feedback turned on, reveals a reduction in the surface $O_3$ concentration by around 2% in the afternoon (16:00 h; local time) when the aerosol-radiation feedback is taken into account.

This study provides a first step to understand the impact of vehicular emissions on the secondary particles formation in the SPMA. Nevertheless, more experimental campaigns are recommended for future work in order to characterize aerosols in

ambient air and to improve their emission estimates so that a better understanding of physical and chemical properties and their formation can be established. This study also evaluates the importance of the VOCs in the formation of not only $O_3$ but also of fine particles. These compounds play an important role concerning health impacts and climate change, and the control of their concentrations requires the description of their formation mechanisms.

## Appendix A

The statistics used in this study are defined as follows:

1. Correlation coefficient (R)

$$R = \frac{\sum_{i=1}^{N}(M_i - \overline{M})(O_i - \overline{O})}{\sqrt{\sum_{i=1}^{N}(M_i - \overline{M})^2}\sqrt{\sum_{i=1}^{N}(O_i - \overline{O})^2}}$$

2. Root mean square error UB ($RMSE_{UB}$)

$$RMSE_{UB} = \sqrt{\frac{1}{N}\sum_{i=1}^{N}[(M_i - \overline{M}) - (O_i - \overline{O})]^2}$$

3. Bias (B)

$$B = \frac{1}{N}\sum_{i=1}^{N}(M_i - O_i)$$

where

$\overline{O} = \frac{1}{N}\sum_{i=1}^{N} O_i$ and $\overline{M} = \frac{1}{N}\sum_{i=1}^{N} M_i$ are the average values of the individual observed and predicted values, $O_i$ and $M_i$, respectively. N is the number of observations.

## 5. Acknowledgments

Prashant Kumar, Angel Vara-Vela and Maria de Fatima Andrade thank the University of Surrey's International Relations Office for the Santander Postgraduate Mobility Award that helped Angel Vara to visit University of Surrey, UK, and develop this research article collaboratively. The authors from Universities of Surrey and Sao Paulo also acknowledge the collaborative funding received through the University Global Partnership Network (UGPN) to the project titled "*Emissions And Role Of Fine Aerosol Particles In Formation Of Clouds and Precipitation (eRAIN) - A demonstration study for the megacity, São Paulo*" for supporting this research work. Maria de Fatima Andrade and Angel Vara-Vela acknowledged funding from the Coordination for the Improvement of Higher Education Personnel (CAPES) and Research Foundation of the State of Sao Paulo (FAPESP, project 2008/58104-8) that allowed the experimental campaigns. The authors also thank the WRF-Chem developers, the NOAA's National Geophysical Data Center, the NCAR's Data Support Section and Atmospheric Chemistry Division, the Latin American Observatory (OLE2), the Sao Paulo Environmental Protection Agency (CETESB), the OpenStreetMap Data Extracts, and the NCAR Command Language (NCL) software for providing the tools and datasets used in this research.

## 6. References

Ackermann, I. J., Hass, H., Memmesheimer, M., Ebel, A., Binkowski, F. S., and Shankar, U.: Modal aerosol dynamics model for Europe: development and first applications, Atmos. Environ., 32, 2981-2999, 1998.

Ahmadov, R., McKeen, S. A., Robinson, A. L., Bahreini, R., Middlebrook, A. M., de Gouw, J. A., Meagher, J., Hsie, E. Y., Edgerton, E., Shaw, S., and Trainer, M.: A volatility basis set model for summertime secondary organic aerosols over the eastern United States in 2006, Journal of Geophysical Research, 117, D06301, doi:10.1029/2011JD016831, 2012.

Albuquerque, T. T. A., Andrade, M. F., and Ynoue, R. Y.: Characterization of atmospheric aerosols in the city of Sao Paulo, Brazil: comparisons between polluted and unpolluted periods, Water Air Soil Pollution, 195, 201-213, 2011.

Anderson, L.: Ethanol fuel use in Brazil: air quality impacts, Energy Environ. Sci., 2, 1015-1037, 2009.

Andrade, M. F., Ynoue, R. Y., Freitas, E. D., Todesco, E., Vara-Vela, A., Ibarra, S., Martins, L. D., Martins, J. A., Carvalho, V. S. B.: Air quality forecasting system for Southeastern Brazil, Front. Environ. Sci., 3, 1-14, 2015.

Andrade, M. F., Fornaro, A., Miranda, R. M., Kerr, A., Oyama, B., Andre, P. A., and Saldiva, P.: Vehicle emissions and $PM_{2.5}$ mass concentrations in six Brazilian cities, Air Quality, Atmosphere and Health, 5, 79-88, 2012.

Binkowski, F. S. and Shankar, U.: The regional particulate matter model, 1. Mode description and preliminary results, Journal of Geophysical Research, 100, 26191-26209, 1995.

Birch, M. E. and Cary, R. A.: Elemental carbon-based method for occupational monitoring of particulate diesel exhaust: methodology and exposure issues, Aerosol Science and Technology, 25, 221-241, 1996.

Brito, J., Rizzo, L. V., Herckes, P., Vasconcellos, P. C., Caumo, S. E. S., Fornaro, A., Ynoue, R. Y., Artaxo, P., and Andrade, M. F.: Physical-chemical

characterisation of the particulate matter inside two road tunnels in the Sao Paulo Metropolitan Area, Atmos. Chem. Phys., 13, 12199-12213, 2013.

Brown, S. G., Lee, T., Roberts, P. T., and Collett, J. L. Jr.: Variations in the OM/OC ratio of urban organic aerosol next to a major roadway, J. Air & Waste Manag. Assoc., 63(12), 1422-1433, 2013.

Carvalho, V. S. B., Freitas, E. D., Martins, L. D., Martins, J. A., Mazzoli, C. R., and Andrade, M. F.: Air quality status and trends over the Metropolitan Area of Sao Paulo, Brazil as a result of emission control policies, Environmental Science & Policy, 47, 68-79, 2015.

Castanho, A. D. A. and Artaxo, P.: Sao Paulo aerosol source apportionment for wintertime and summertime, Atmos. Environ., 35, 4889-4902, 2001.

Costa, R. C. and Sodré, J. R.: Hydrous ethanol vs. gasoline-ethanol blend: Engine performance and emissions, Fuel, 89, 287-293, 2010.

CETESB-Companhia de Tecnologia de Saneamento Ambiental. Relatorio Anual de Qualidade do Ar no Estado de Sao Paulo 2012, Sao Paulo, 2013.

CETESB-Companhia de Tecnologia de Saneamento Ambiental. Emissões veiculares no Estado de São Paulo 2011, Sao Paulo, 2012.

CETESB-Companhia de Tecnologia de Saneamento Ambiental. Relatorio Anual de Qualidade do Ar no Estado de Sao Paulo 2009, Sao Paulo, 2010.

Chang, J. S., Binkowki, F. S., Seaman, N. L., McHenry, J. N., Samson, P. J., Stockwell, W. R., Walcek, C. J., Madronich, S., Middleton, P. B., Pleim, J. E., and Lansford, H. H.: The regional acid deposition model and engineering model, State-of-Science/Technology, Report 4, National Acid Precipitation Assessment Program, Washington, DC, 1989.

732 Draxler, R. R. and Hess, G. D.: An overview of the HYSPLIT 4 modelling system of
733 trajectories, dispersion, and deposition, Aust. Meteor. Mag., 47, 295-308, 1998.
734 Emmons, L. K., Walters, S., Hess, P. G., Lamarque, F., Pfister, G. G., Fillmore, D.,
735 Granier, C., Guenther, A., Kinnison, D., Laepple, T., Orlando, J., Tie, X.,
736 Tyndall, G., Wiedinmyer, C., Baughcum, S. L., and Kloster, S.: Description
737 and evaluation of the Model for Ozone and Related chemical Tracers, version
738 4 (MOZART-4), Geosci. Model Dev., 3, 43-67, 2010.
739 Ginoux, P., Chin, M., Tegen, I., Prospero, J. M., Holben, B., Dubovik, O., and Lin,
740 S-J.: Sources and distributions of dust aerosols simulated with the GOCART
741 model, Journal of Geophysical Research, 106, 20,255-20,273, 2001.
742 Gong, S. L.: A parameterization of sea-salt aerosol source function for sub- and super-
743 micron particles, Global Biogeochemical Cycles, 17, 1097,
744 doi:10.1029/2003GB002079, 2003.
745 Gorin, C. A., Collett, J. L. Jr., and Herckes, P.: Wood smoke contribution to winter
746 aerosol in Fresno, CA, J. Air & Waste Manag. Assoc., 56(11), 1584-1590,
747 2006.
748 GrEC-Grupo de Estudos Climáticos. Relatório climatológico mensal, previsão climática
749 para o Brasil: Set-Out-Nov/2012, Sao Paulo, 2012a. Available at:
750 www.grec.iag.usp.br/link_grec_old/relatorios_climatologicos/2012/agosto/.
751 GrEC-Grupo de Estudos Climáticos. Relatório climatológico mensal, monitoramento
752 climático para o Brasil: Set/2012, Sao Paulo, 2012b. Available at:
753 www.grec.iag.usp.br/link_grec_old/relatorios_climatologicos/2012/setembro/.
754 Grell, G. A., Peckham, S. E., Schmitz, R., McKeen, S. A., Wilczak, J., and Eder, B.:
755 Fully coupled “online” chemistry within the WRF model, Atmos. Environ., 39,
756 6957-6975, 2005.

Guenther, A. B., Zimmerman, P. R., Harley, P. C., Monson, R. K., and Fall, R.: Isoprene and monoterpene emission rate variability: model evaluations and sensitivity analyses, Journal of Geophysical Research, 98D, 12609-12617, 1993.

Guenther, A., Zimmerman, P., and Wildermuth, M.: Natural volatile organic compound emission rateestimates for US woodland landscapes, Atmos. Environ., 28, 1197-1210, 1994.

Fast, J. D., Gustafson, W. I., Easter, R. C., Zaveri, R. A., Barnard, J. C., Chapman, E. G., Grell, G. A., and Peckham, S. E.: Evolution of ozone, particulates, and aerosol direct radiative forcing in the vecinity of Houston using a fully coupled meteorology-chemistry-aerosol module, Journal of Geophysical Research, 111, D21305, doi:10.1029/2005JD006721, 2006.

Forkel, R., Werhahn, J., Hansen, A. B., McKeen, S., Peckham, S., Grell, G., and Suppan, P.: Effect of aerosol-radiation feedback on regional air quality - A case study with WRF/Chem, Atmospheric Environment, 53, 202-211, 2012.

Heal, M. R., Kumar, P., and Harrison, R. M.: Particles, air quality, policy and health, Chem. Soc. Rev., 41, 6606-6630, 2012.

Jenkin, M. E. and Clemitshaw, K. C.: Ozone and other secondary photochemical pollutants: chemical processes governing their formation in the planetary boundary layer, Atmos. Environ., 34, 2499-2527, 2000.

Kroll, J. H. and Seinfeld, J. H.: Chemistry of secondary organic aerosol: Formation and evolution of low-volatility organics in the atmosphere, Atmos. Environ., 42, 3593-3624, 2008.

780 Kulmala, M., Laaksonen, A., and Pirjola, L.: Parameterization for sulphuric
781 acid/water nucleation rates, Journal of Geophysical Research, 103, 8301-
782 8307, 1998.
783 Kumar, P., Morawska, L., Birmili, W., Paasonen, P., Hu, M., Kulmala, M., Harrison,
784 R.M., Norford, L., and Britter, R.: Ultrafine particles in cities, Environment
785 International, 66, 1-10, 2014.
786 Kumar, P., Robins, A., Vardoulakis, S., and Britter, R.: A review of the characteristics
787 of nanoparticles in the urban atmosphere and the prospects for developing
788 regulatory control, Atmos. Environ., 44, 5035-5052, 2010.
789 Kumar, P., Ketzel, M., Vardoulakis, S., Pirjola, L., Britter, R.: Dynamics and dispersion
790 modelling of nanoparticles from road traffic in the urban atmospheric
791 environment - a review, J. Aerosol Sci., 42, 580-603, 2011.
792 Li, G., Bei, N., Tie, X., and Molina, L. T.: Aerosol effects on the photochemistry in
793 Mexico City during MCMA-2006/MILAGRO campaign, Atmos. Chem. Phys.,
794 11, 5169-5182, 2011a.
795 Li, G., Zavala, M., Lei, W., Tsimpidi, A. P., Karydis, V. A., Pandis, S. N.,
796 Canagaratna, M. R., and Molina, L. T.: Simulations of organic aerosol
797 concentrations in Mexico City using the WRF-Chem model during the
798 MCMA-2006/MILAGRO campaign, Atmos. Chem. Phys., 11, 3789-3809,
799 2011b.
800 Li, G., Zhang, R., and Fan, J.: Impacts of black carbon aerosol on photolysis and
801 ozone, Journal of Geophysical Research, 110, D23206,
802 doi:10.1029/2005JD005898, 2005.
803 Marple, V. A., Rubow, K. L., Ananth, G. P., and Fissan, H. J.: Micro-Orifice Uniform
804 Deposit Impactor, Journal of Aerosol Science, 17, 489-494, 1986.

Martins, L. D., Vasconcellos, P. C., Carvalho, L. F., Andrade, M. F.: Estimated impact of biogenic hydrocarbon emissions on photochemical oxidant formation in Sao Paulo during two periods of the winters of 1999-2000, Revista Brasileira de Meteorologia, 21, 190-200, 2006.

McMurry, P., Shepherd, M., and Vickery, J.: Particulate Matter Science for Policy Makers: A NARSTO Assessment, Cambridge University Press, Cambridge, England, 2004.

Middleton, P., Stockwell, W. R., and Carter, W. P. L.: Aggregation and analysis of volatile organic compound emissions for regional modelling, Atmos. Environ., 24A, 1107-1133, 1990.

Miranda, R. M. and Andrade, M. F.: Physicochemical characteristics of atmospheric aerosols during winter in the Sao Paulo Metropolitan Area in Brazil, Atmos. Environ., 39, 6188-6193, 2005.

Monahan, E. C., Spiel, D. E., Davidson, K. L.: A model of marine aerosol generation via whitecaps and wave disruption. In: Monahan, E. C., MacNiocaill, G. D. (Eds.), Oceanic Whitecaps. Reidel Publishing Company, Norwell, Mass, 167-174, 1986.

Muñoz, A. G., López, P., Velásquez, R., Monterrey, L., León, G., Ruiz, F., Recalde, C., Cadena, J., Mejía, R., Paredes, M., Bazo, J., Reyes, C., Carrasco, G., Castellón, Y., Villarroel, C., Quintana, J., and Urdaneta, A.: An Environmental Watch System for the Andean Countries: El Observatorio Andino, Bull. Amer. Meteor. Soc., 91, 1645-1652, 2010.

Muñoz, A. G., Ruiz-Carrascal, D., Ramírez, P., León, G., Quintana, J., Bonilla, A., Torres, W., Pastén, M., and Sánchez, O.: Risk Management at the Latin

American Observatory, in: Risk Management–Current Issues and Challenges, InTech Publications, doi:10.5772/50788, 533-556, 2012.

Nogueira, T., Dominutti, P. A., De Carvalho, L. R. F., Fornaro, A., and Andrade, M. F.: Formaldehyde and acetaldehyde measurements in urban atmosphere impacted by the use of ethanol biofuel: Metropolitan Area of Sao Paulo, 2012-2013, Fuel, 134, 505-513, 2014.

Odum, J. R., Hoffmann, T., Bowman, F., Collins, D., Flagan, R. C., and Seinfeld, J. H.: Gas/particle partitioning and secondary organic aerosol yields, Environmental Science Technology, 30, 2580-2585, 1996.

Pankow, J. F.: An absorption model of the gas aerosol partitioning involved in the formation of secondary organic aerosol, Atmos. Environ., 28, 185-188, 1994a.

Pankow, J. F.: An absorption model of the gas aerosol partitioning involved in the formation of secondary organic aerosol, Atmos. Environ., 28, 189-93, 1994b.

Pérez-Martínez, P. J., Andrade, M. F., and Miranda, R. M.: Traffic-related air quality trends in Sao Paulo, Brazil, J. Geophys. Res. Atmos., 120, 6290-6304, doi:10.1002/2014JD022812, 2015.

Pérez-Martínez, P. J., Miranda, R. M., Nogueira, T., Guardani, M. L., Fornaro, A., Ynoue, R., and Andrade, M. F.: Emission factors of air pollutants from vehicles measured inside road tunnels in Sao Paulo: case study comparison, Int. J. Environ. Sci. Technol., 11, 2155-2168, 2014.

Real, E. and Sartelet, K.: Modelling of photolysis rates over Europe: impact on chemical gaseous species and aerosols, Atmos. Chem. Phys., 11, 1711-1727, 2011.

852 Salvo, A. and Geiger, F. M.: Reduction in local ozone levels in urban Sao Paulo due to
853 a shift from ethanol to gasoline use, Nature Geoscience, 7, 450-458,
854 doi:10.1038/ngeo2144, 2014.
855 Saxena, P., Hudischewskyj, A. B., Seigneur, C., and Seinfeld, J. H.: A comparative
856 study of equilibrium approaches to the chemical characterization of
857 secondary aerosols, Atmos. Environ., 20, 1471-1483, 1986.
858 Schell, B., Ackerman, I. J., Hass, H., Binkowski, F. S., and Ebel, A.: Modelling the
859 formation of secondary organic aerosol within a comprehensive air quality
860 model system, Journal of Geophysical Research, 106, 28275-28293, 2001.
861 Seinfeld, J. H. and Pandis, S. N.: Atmospheric Chemistry and Physics: from air
862 pollution to climate change, Second Edition, Jhon Wiley, New Jersey,
863 2006.
864 Shrivastava, M., Berg, L. K., Fast, J. F., Easter, R. C., Laskin, A., Chapman, E. G.,
865 Gustafson Jr, W. I., Liu, Y., and Berkowitz, C. M.: Modelling aerosols and
866 their interactions with shallow cumuli during the 2007 CHAPS field study,
867 Journal of Geophysical Research: Atmospheres, 118, 1343-1360, 2013.
868 Taylor, K. E.: Summarizing multiple aspects of model performance in a single diagram,
869 Journal of Geophysical Research, 106(D7), 7183-7192,
870 doi:10.1029/2000JD900719, 2001.
871 Tuccella, P., Curci, G., Visconti, G., Bessagnet, B., Menut, L., and Park, R. J.:
872 Modelling of gas and aerosol with WRF-Chem over Europe: Evaluation and
873 sensitivity study, Journal of Geophysical Research, 117, D03303,
874 doi:10.1029/2011JD016302, 2012.
875 Vasconcellos, P. C., Souza, D. Z., Sanchez-Ccoyllo, O. R., Bustillos, J. O. V., Lee,
876 H., Santos, F. C., Nascimento, K. H., Araujo, M. P., Saarnio, K., Teinila, K.,

877 and Hillamo, R.: Determination of anthropogenic and biogenic
878 compounds on atmospheric aerosol collected in urban, biomass burning
879 and forest areas in Sao Paulo, Brazil, Science of the Total Environment, 408,
880 5836-5844, 2010.
881 Vieira-Filho, M. S., Pedrotti, J. J., and Fornaro, A.: Contribution of long and mid-
882 range transport on the sodium and potassium concentrations in rainwater samples,
883 Sao Paulo megacity, Brazil, Atmos. Environ., 79, 299-307, 2013.
884 Wedding, J. B., Weigand, M., John, W., and Wall, S.: Sampling effectiveness of the
885 inlet to the dichotomous sampler, Environ. Sci. Technol., 14(11), 1367-1370, 1980.
886 Ynoue, R. Y. and Andrade, M. F.: Size-resolved mass balance of aerosol particles over
887 the Sao Paulo Metropolitan Area of Brazil, Aerosol Science and Technology, 1,
888 52-62, 2004.
889

890 Table 1. Description of aerosol sampling campaigns performed at IAG-USP.

| Parameter | Sampling frequency | Period of sampling | Sampling device |
|---|---|---|---|
| Aerosol mass size distribution | 24 hours | July-September | MOUDI impactor |
| $PM_{2.5}$ and $PM_{10}$ concentration | 12 hours | July-September | Dichotomous sampler |
| OC and EC concentration | 12 hours | August-September | Sunset OC-EC analyser |

891
892

Table 2. Description of measurement sites.

| Initials | Name | Latitude | Longitude | Measured species |
|---|---|---|---|---|
| NSO | Nossa S. do O | -23.4796 | -46.6916 | $PM_{10}$, $O_3$ |
| SAN | Santana | -23.5055 | -46.6285 | $PM_{10}$ |
| PDP | Parque D. Pedro | -23.5448 | -46.6276 | $PM_{10}$, $O_3$ |
| MOO | Mooca | -23.5497 | -46.5984 | $PM_{10}$, $O_3$ |
| CCE | Cerqueira Cesar | -23.5531 | -46.6723 | $PM_{10}$ |
| IAG-USP | IAG-USP | -23.5590 | -46.7330 | $PM_{10}$, $PM_{2.5}$, OC, EC Aerosol mass size distrib.[a] |
| IPEN-USP | IPEN-USP | -23.5662 | -46.7374 | $PM_{2.5}$, $O_3$, NOx, CO |
| IBI | Ibirapuera | -23.5914 | -46.6602 | $PM_{10}$, $O_3$, NOx, CO |
| CON | Congonhas | -23.6159 | -46.6630 | $PM_{10}$, $PM_{2.5}$ |
| AF-IAG | AF-IAG | -23.6500 | -46.6167 | T, RH, WS, WD[b] |
| SAM | Santo Amaro | -23.6545 | -46.7095 | $PM_{10}$ |
| INT | Interlagos | -23.6805 | -46.6750 | $PM_{10}$, $O_3$, T, RH, WS, WD |

[a]includes $SO_4^{2-}$, $NO_3^-$, $NH_4^+$, $Na^+$, $Cl^-$ and $PM_{10}$.

[b]T, RH, WS, and WD denote temperature, relative humidity, wind speed and wind direction, respectively.

898 Table 3. Selected WRF-Chem configuration options.

| Atmospheric Process | WRF-Chem option |
|---|---|
| Longwave radiation | RRTM |
| Shortwave radiation | Goddard |
| Surface layer | Monin-Obukhov |
| Land surface | Noah |
| Boundary layer | YSU |
| Cumulus clouds[a] | Grell 3D |
| Cloud microphysics | Lin |
| Gas-phase chemistry | RADM2 |
| Aerosol chemistry | MADE/SORGAM |
| Photolysis | Fast-J |

899 [a]Outer domains only

900

Table 4. Description of WRF-Chem simulations.

| Label | Description |
|---|---|
| Case_0 | Emission of gases |
| (Baseline simulation) | Emission of aerosols |
| | Aerosol-radiation feedback turned on |
| Case_1 | Emission of gases |
| | No emission of aerosols |
| | Aerosol-radiation feedback turned on |
| Case_2 | Emission of gases |
| | Emission of aerosols |
| | Aerosol-radiation feedback turned off |

904 Table 5. Performance statistics for WRF-Chem predictions at all sites[a]

| Index | $PM_{2.5}$ | $PM_{10}$ | $O_3$ | NOx | CO | T | RH | U[b] | V[c] |
|---|---|---|---|---|---|---|---|---|---|
| R | 0.73 | 0.72 | 0.63 | 0.42 | 0.54 | 0.71 | 0.62 | 0.48 | 0.44 |
| B | -8.84 | -14.1 | -0.85 | -8.75 | -0.27 | 0.65 | -5.74 | -0.96 | 0.75 |
| $RMSE_{UB}$ | 6.83 | 10.59 | 27.45 | 30.35 | 0.57 | 3.21 | 20.06 | 1.04 | 1.02 |

905 [a]Values are averaged from all the individual indexes found at the measurement sites.

906 Individual indexes are calculated from both hourly observed and predicted values.

907 [b]Zonal wind component

908 [c]Meridional wind component

909

910 Figure 1. Downtown area of the 3 km modelling domain (d03) showing the locations of
911 measurement sites and WRF topography in the vicinity of SPMA. Red dots
912 represent sites with information on $O_3$ and PM. Yellow dots represent only
913 sites with information on PM. Blue dot represents the location of the IAG-
914 USP's climatological station.
915 Figure 2. Emission rates for Aromatic VOCs at 19 UTC in the 3 km modelling
916 domain.
917 Figure 3. Hourly accumulated precipitation and relative humidity observed at the
918 IAG-USP's climatological station during the study period.
919 Figure 4. HYSPLIT three-day backward trajectories and locations of fires in Sao Paulo
920 State and part of central-west region of Brazil. Pink markers represent the
921 observed fire locations during the study period considering different satellite
922 products (GOES, AQUA, TERRA, NOAA). The backward trajectories starting
923 at IAG-USP were calculated for the days 9 and 31 August and 5 September 2012
924 at three different altitudes: 500 m (red lines), 1000 m (blue lines), and 2000 m
925 (green lines).
926 Figure 5. Daily (top), diurnal (bottom), and nocturnal (middle) mean concentrations for
927 EC, OC, $PM_{10}$, $PM_{2.5-10}$, $PM_{2.5}$ (left panels), and Na, $Fe_2SO_3$, $SiO_2$, $K_2O$, and S
928 (right panels). The $PM_{2.5-10}$ aerosol variable is defined as particulate matter with
929 aerodynamic diameter between 2.5 and 10 μm. The grey line indicates the WHO
930 air quality standard for PM2.5 (25 μg $m^{-3}$).
931 Figure 6. The predicted average of wind vectors at 10 m and temperature at 2 m from
932 the baseline simulation (Case_0) for the whole study period in the 3 km
933 modelling domain. Blue dots represent the locations of the measurement sites,

whereas cyan numbers represent the observed average temperature in those sites: 17.7 °C in AF-IAG and 17.8 °C in INT.

Figure 7. The observed and predicted daily variations of $PM_{2.5}$ concentrations at three sites in SPMA for the 3 km modelling domain.

Figure 8. The observed and predicted daily variations of $PM_{10}$ concentrations at ten sites in SPMA for the 3 km modelling domain.

Figure 9. The observed and predicted hourly variations of $O_3$ concentrations at six sites in SPMA for the 3 km modelling domain.

Figure 10. Taylor diagram showing the individual correlation coefficients, biases, and normalized standard deviations for the $PM_{2.5}$, $PM_{10}$, and $O_3$ concentrations.

Figure 11. The predicted average surface distribution of $PM_{2.5}$ concentrations for the whole study period in the 3 km modelling domain. Red dots represent the locations of the measurement sites with information on $PM_{2.5}$, whereas cyan numbers represent the observed average $PM_{2.5}$ concentration in those sites: 23.4 μg $m^{-3}$ in IPEN-USP, 21.3 μg $m^{-3}$ in IAG-USP, and 22.2 μg $m^{-3}$ in CON.

Figure 12. The predicted average surface distribution of $PM_{10}$ concentrations for the whole study period in the 3 km modelling domain. Red dots represent the locations of the measurement sites with information on $PM_{10}$, whereas cyan numbers represent the observed average $PM_{10}$ concentration in those sites: 49.5 μg $m^{-3}$ in IAG-USP and 38.7 μg $m^{-3}$ in CON.

Figure 13. The predicted average surface distribution of the $PM_{2.5}$:$PM_{10}$ ratio for the whole study period in the 3 km modelling domain. Red dots represent the locations of the measurement sites with information on both $PM_{2.5}$ and $PM_{10}$, whereas cyan numbers represent the observed average $PM_{2.5}$:$PM_{10}$ ratio in those sites: 0.43 in IAG-USP and 0.57 in CON.

959 Figure 14. The observed and predicted daily variations of OC and EC concentrations
960 at IAG-USP.
961 Figure 15. The observed and predicted average aerosol mass size distribution for $SO_4$,
962 $NO_3$, $NH_4$, Na, Cl, and other $PM_{10}$ constituents at IAG-USP. The observed
963 aerosol distributions were collected in ten size classes using a rotated impactor
964 (MOUDI) and joined adequately according to the three modes used by the
965 MADE aerosol scheme: Aitken (<0.1 μm), accumulation (0.1-1 μm) and coarse
966 (>1 μm). The five inorganic ions carried in MADE are only calculated for the
967 Aitken and accumulation modes. The WRF's $PM_{10}$ aerosol variable does not
968 include neither OC nor EC for this comparison.
969 Figure 16. The observed and predicted average contributions for the main identified
970 constituents of $PM_{2.5}$ at IAG-USP.
971 Figure 17. The impact of (a) emissions of primary gases on the fine particles formation,
972 (b) emissions of dust-sea salt aerosols on the $PM_{10}$ concentration, and (c) aerosol
973 direct effect on the ground level $O_3$ concentrations at 16:00 h (local time).
974

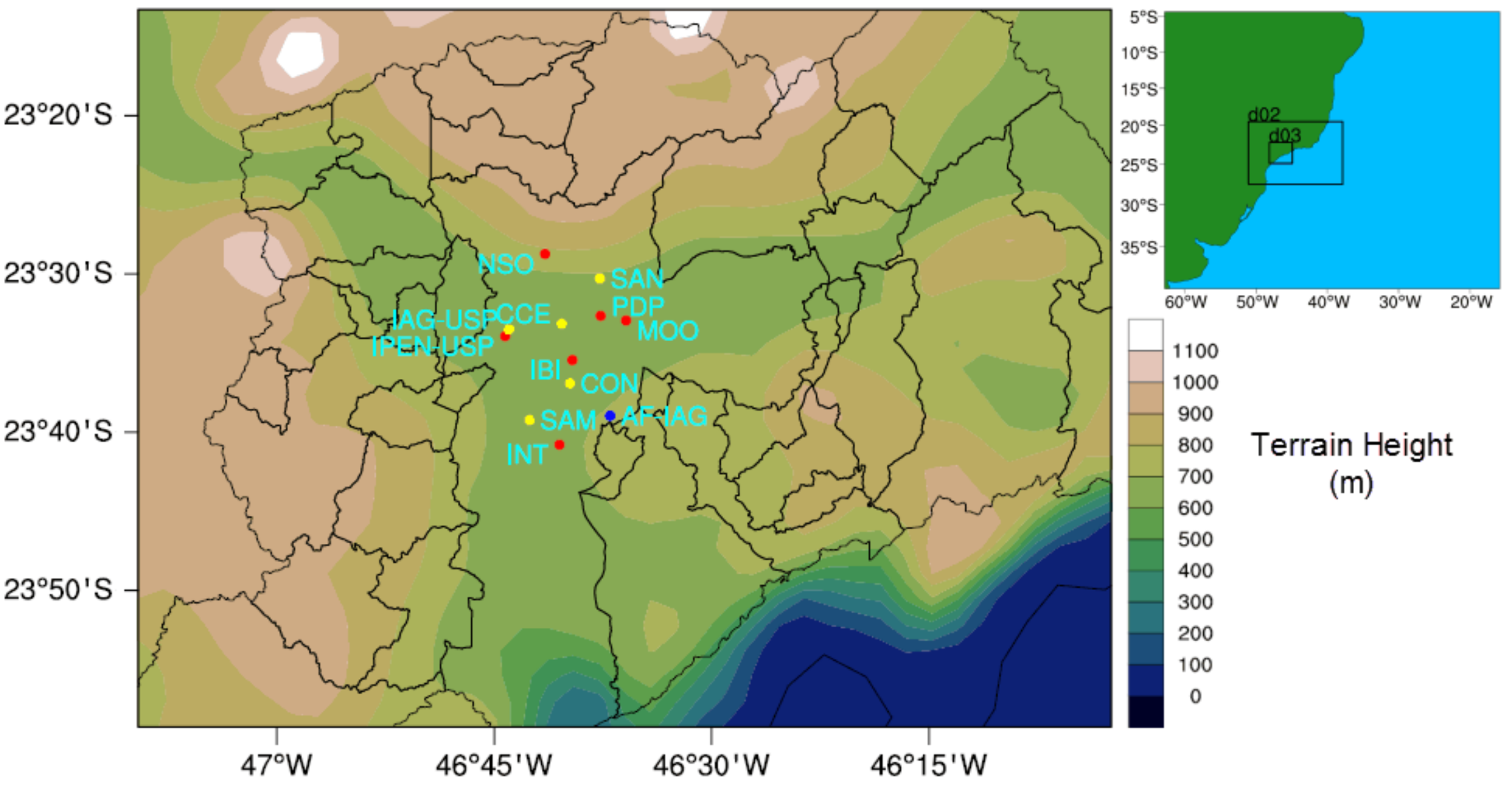
23°20'S
23°30'S
23°40'S
23°50'S
47°W
46°45'W
46°30'W
46°15'W
NSO
SAN
PDP
MOO
IAG-USP
CCE
IPEN-USP
IBI
CON
SAM
AF-IAG
INT
5°S
10°S
15°S
20°S
25°S
30°S
35°S
60°W
50°W
40°W
30°W
20°W
d02
d03
1100
1000
900
800
700
600
500
400
300
200
100
0
Terrain Height
(m)

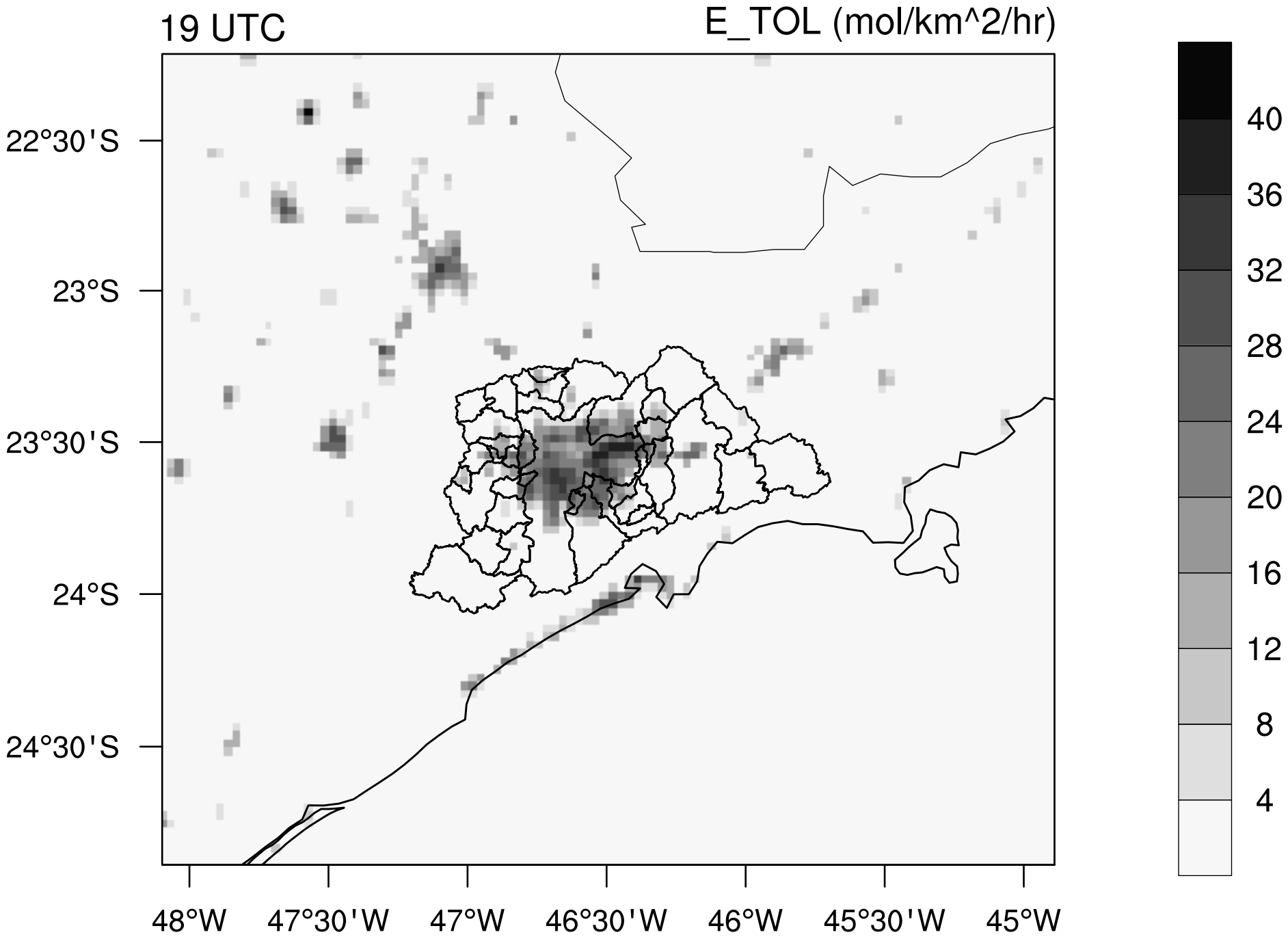
19 UTC
E_TOL (mol/km^2/hr)
22°30'S
23°S
23°30'S
24°S
24°30'S
48°W
47°30'W
47°W
46°30'W
46°W
45°30'W
45°W
40
36
32
28
24
20
16
12
8
4

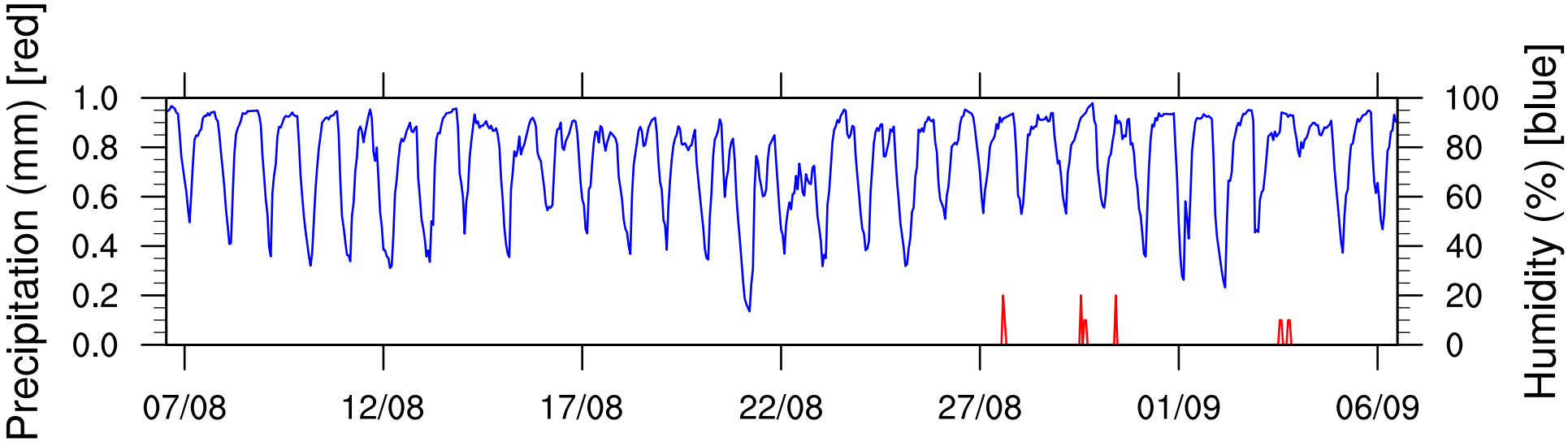
Precipitation (mm) [red]
1.0
0.8
0.6
0.4
0.2
0.0
100
80
60
40
20
0
Humidity (%) [blue]
07/08
12/08
17/08
22/08
27/08
01/09
06/09

8/9/2012 3 tarde/noite

HYSPLIT

Minas Gerais

Espírito Santo

Mato Grosso do Sul

09/02/2012 18 UTC - 500 m

09/02/2012 18 UTC - 2000 m

Rio de Janeiro

09/02/2012 18 UTC - 1000 m

08/06/2012 18 UTC - 500 m

08/06/2012 18 UTC - 2000 m

Paraguai

Assunção

Paraná

Itapúa

Chaco

Santa Catarina

Iberá Wetlands

Rio Grande do Sul

Lagoa dos Patos

Rivera

Uruguai

Lagoa Mirim

08/28/2012 18 UTC - 500 m

08/28/2012 18 UTC - 1000 m

Monitoramento de Queimadas

Legendas
- Goes
- Aqua
- Terra
- MModis-01D
- NOAA-12
- NOAA-12D
- NOAA-14
- NOAA-15
- NOAA-15D
- NOAA-17
- NOAA-18
- NOAA-18D
- Meteosat

Image Landsat
© 2015 Google
Data SIO, NOAA, U.S. Navy, NGA, GEBCO
US Dept of State Geographer

Google earth

Data das imagens: 4/9/2013 lat -25.364396° lon -46.185469° elev -108 m altitude do ponto de visão 2297.00 km

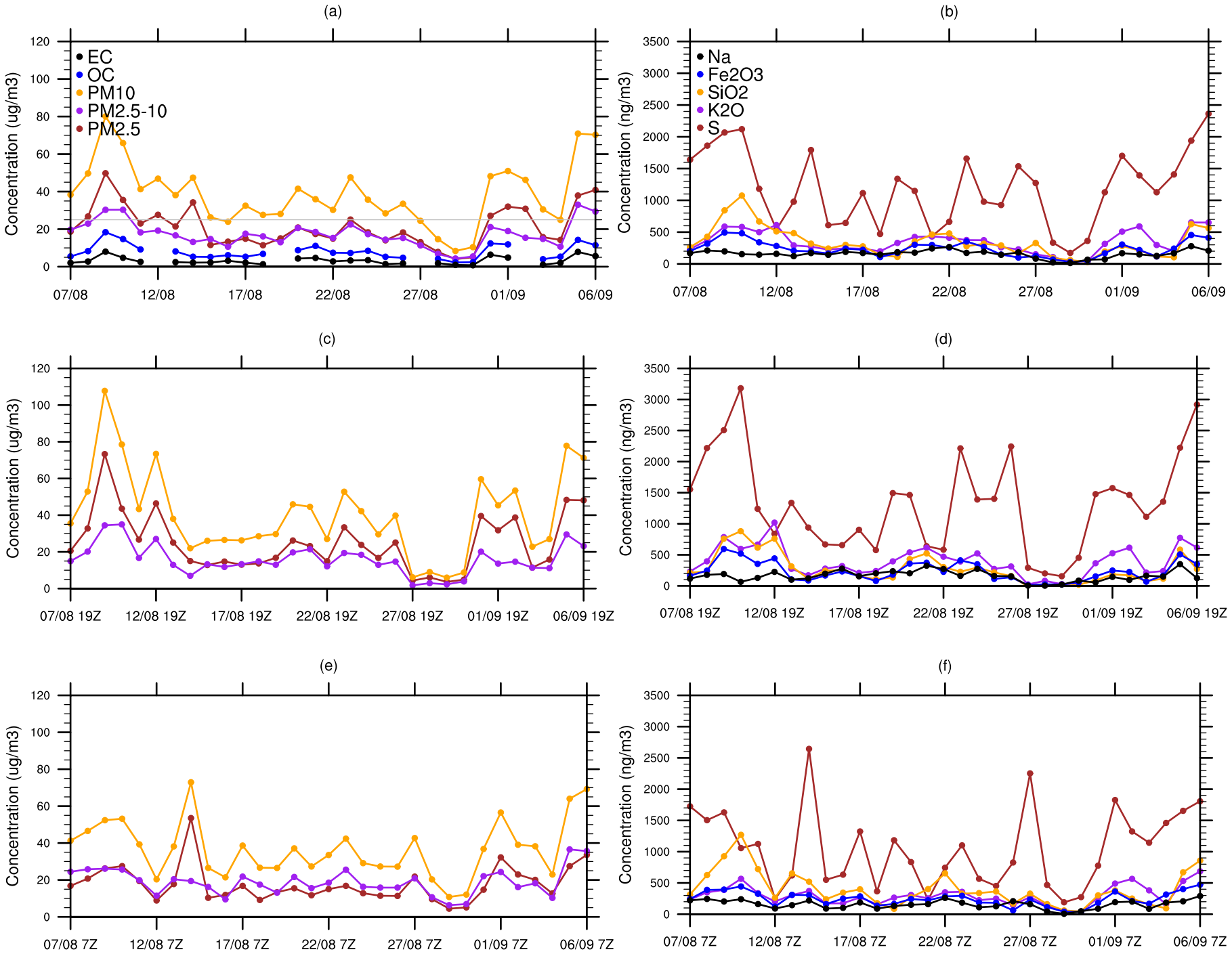
(a)
Concentration (ug/m3)
EC
OC
PM10
PM2.5-10
PM2.5
07/08
12/08
17/08
22/08
27/08
01/09
06/09
(b)
Concentration (ng/m3)
Na
Fe2O3
SiO2
K2O
S
(c)
Concentration (ug/m3)
07/08 19Z
12/08 19Z
17/08 19Z
22/08 19Z
27/08 19Z
01/09 19Z
06/09 19Z
(d)
Concentration (ng/m3)
(e)
Concentration (ug/m3)
07/08 7Z
12/08 7Z
17/08 7Z
22/08 7Z
27/08 7Z
01/09 7Z
06/09 7Z
(f)
Concentration (ng/m3)

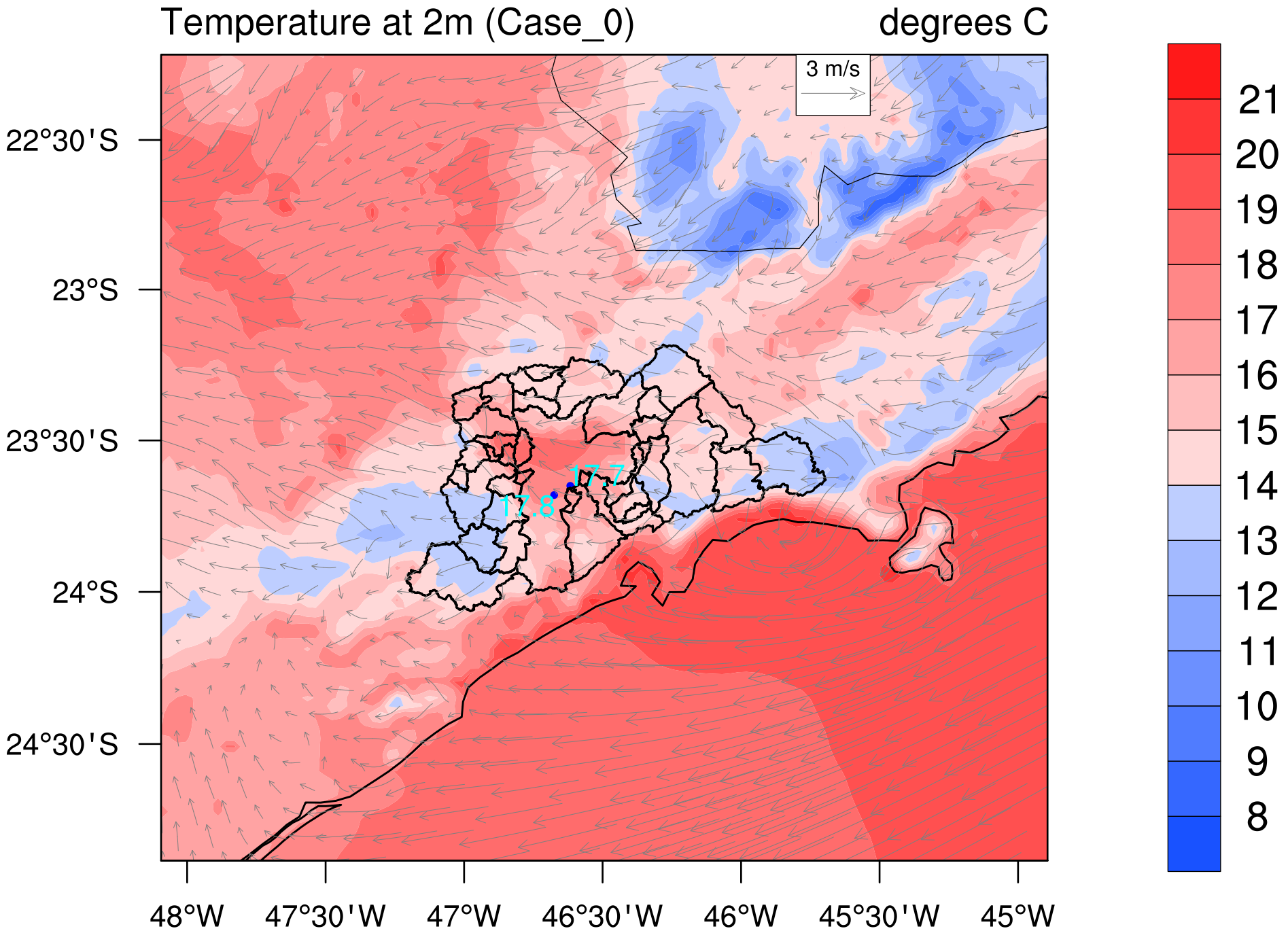
Temperature at 2m (Case_0)
degrees C
3 m/s
22°30'S
23°S
23°30'S
24°S
24°30'S
48°W
47°30'W
47°W
46°30'W
46°W
45°30'W
45°W
17.7
17.8
21
20
19
18
17
16
15
14
13
12
11
10
9
8

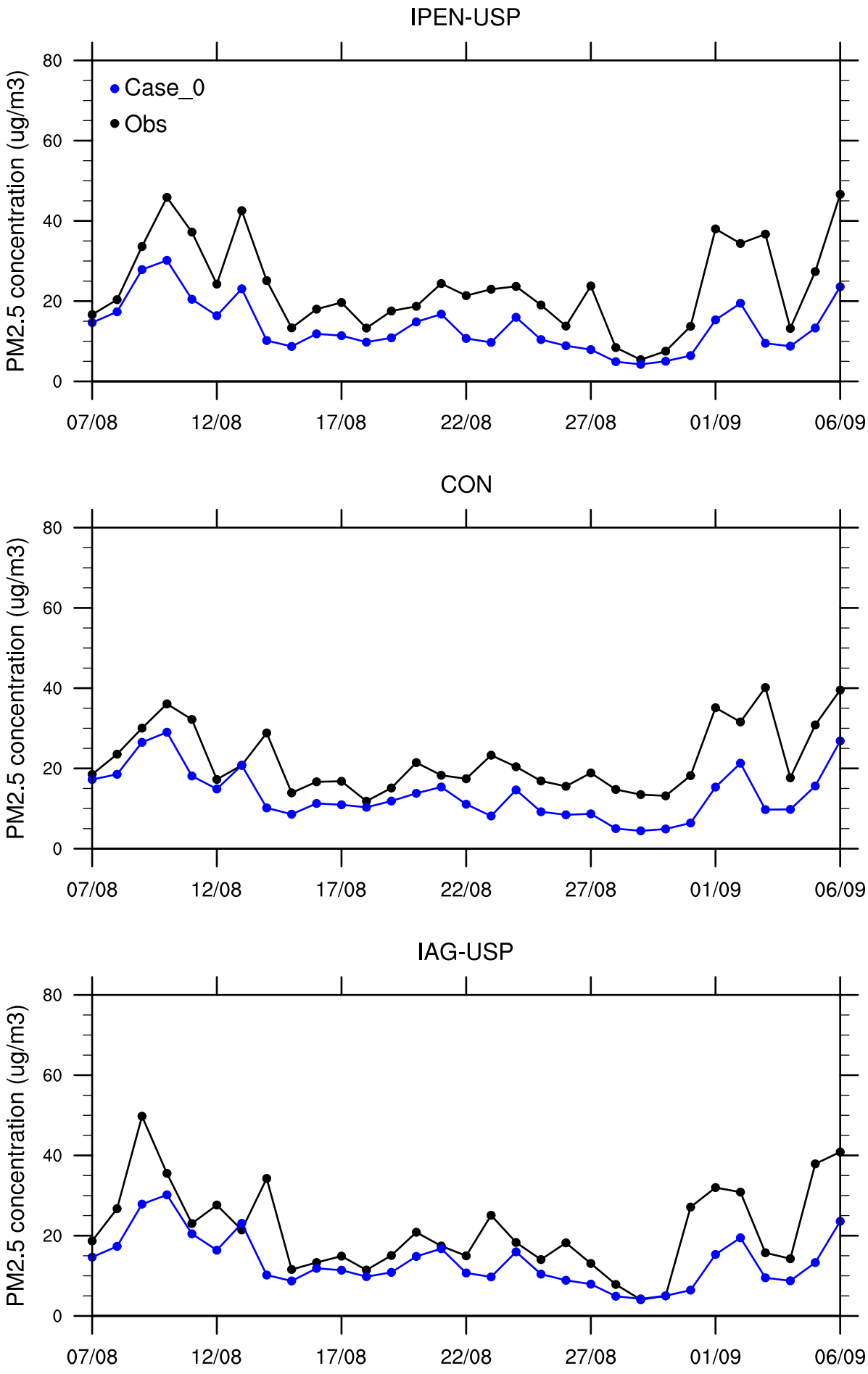
IPEN-USP
Case_0
Obs
PM2.5 concentration (ug/m3)
0
20
40
60
80
07/08
12/08
17/08
22/08
27/08
01/09
06/09
CON
PM2.5 concentration (ug/m3)
0
20
40
60
80
07/08
12/08
17/08
22/08
27/08
01/09
06/09
IAG-USP
PM2.5 concentration (ug/m3)
0
20
40
60
80
07/08
12/08
17/08
22/08
27/08
01/09
06/09

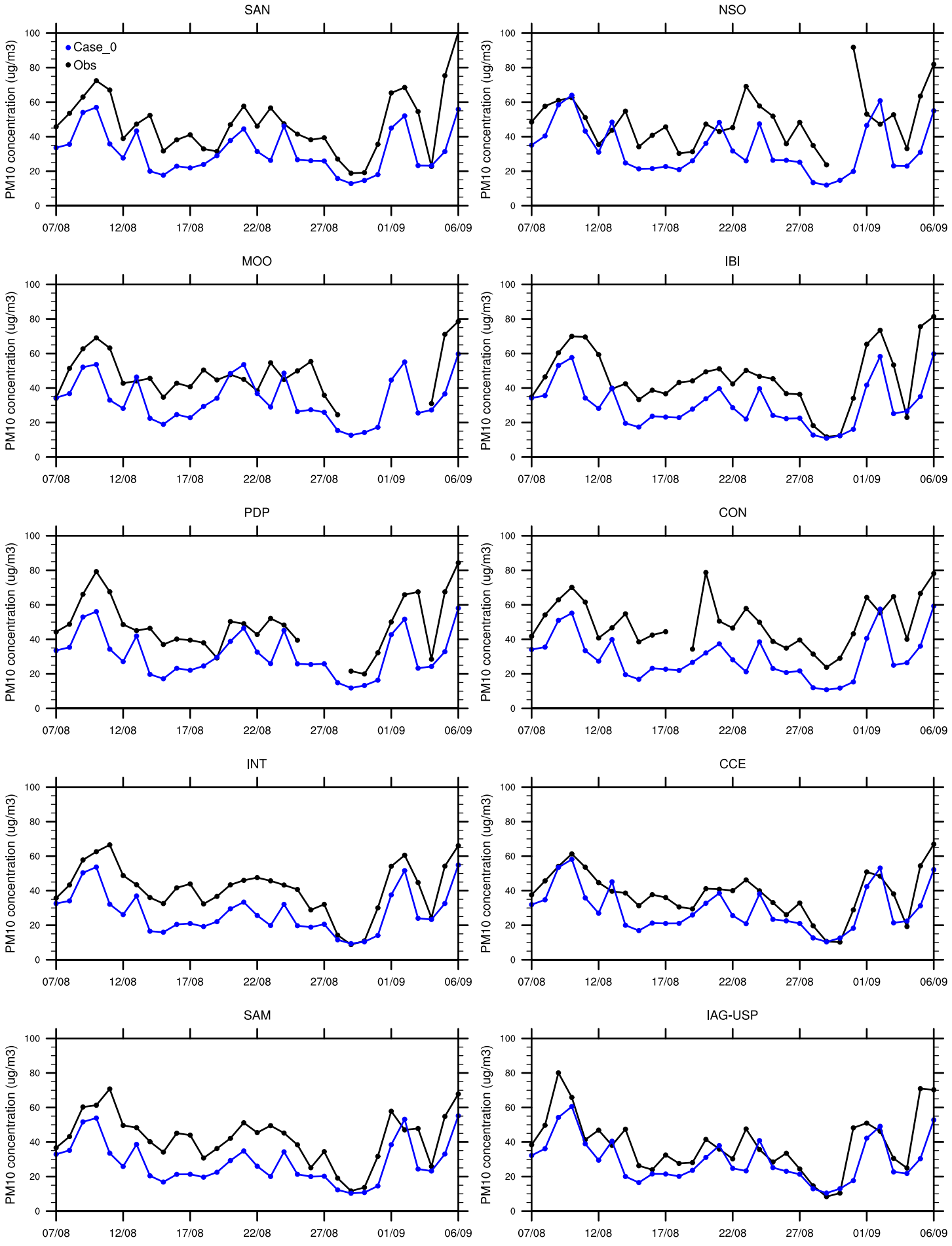
SAN
NSO
MOO
IBI
PDP
CON
INT
CCE
SAM
IAG-USP
Case_0
Obs
PM10 concentration (ug/m3)
0
20
40
60
80
100
07/08
12/08
17/08
22/08
27/08
01/09
06/09

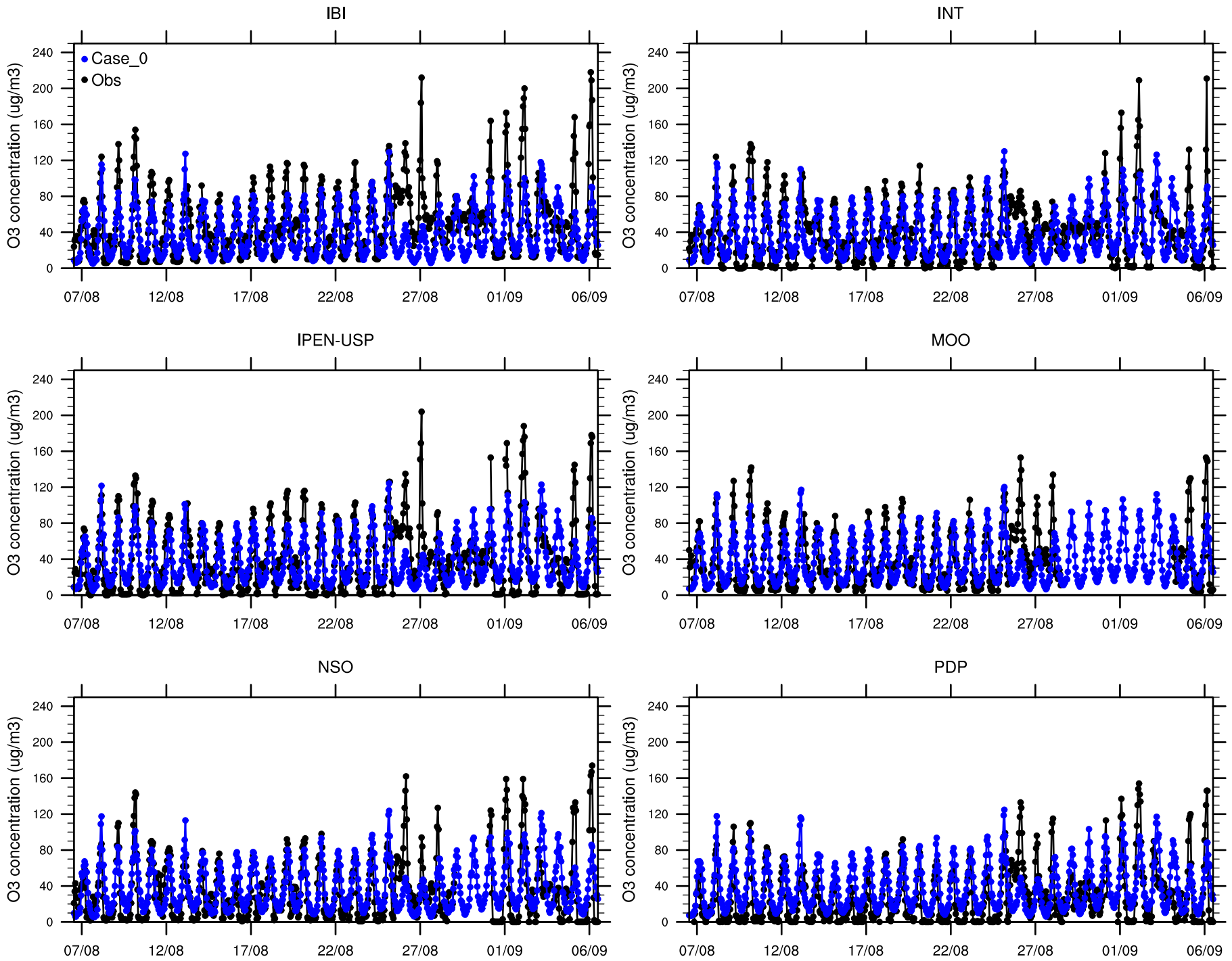
IBI
INT
IPEN-USP
MOO
NSO
PDP
Case_0
Obs
O3 concentration (ug/m3)
0
40
80
120
160
200
240
07/08
12/08
17/08
22/08
27/08
01/09
06/09

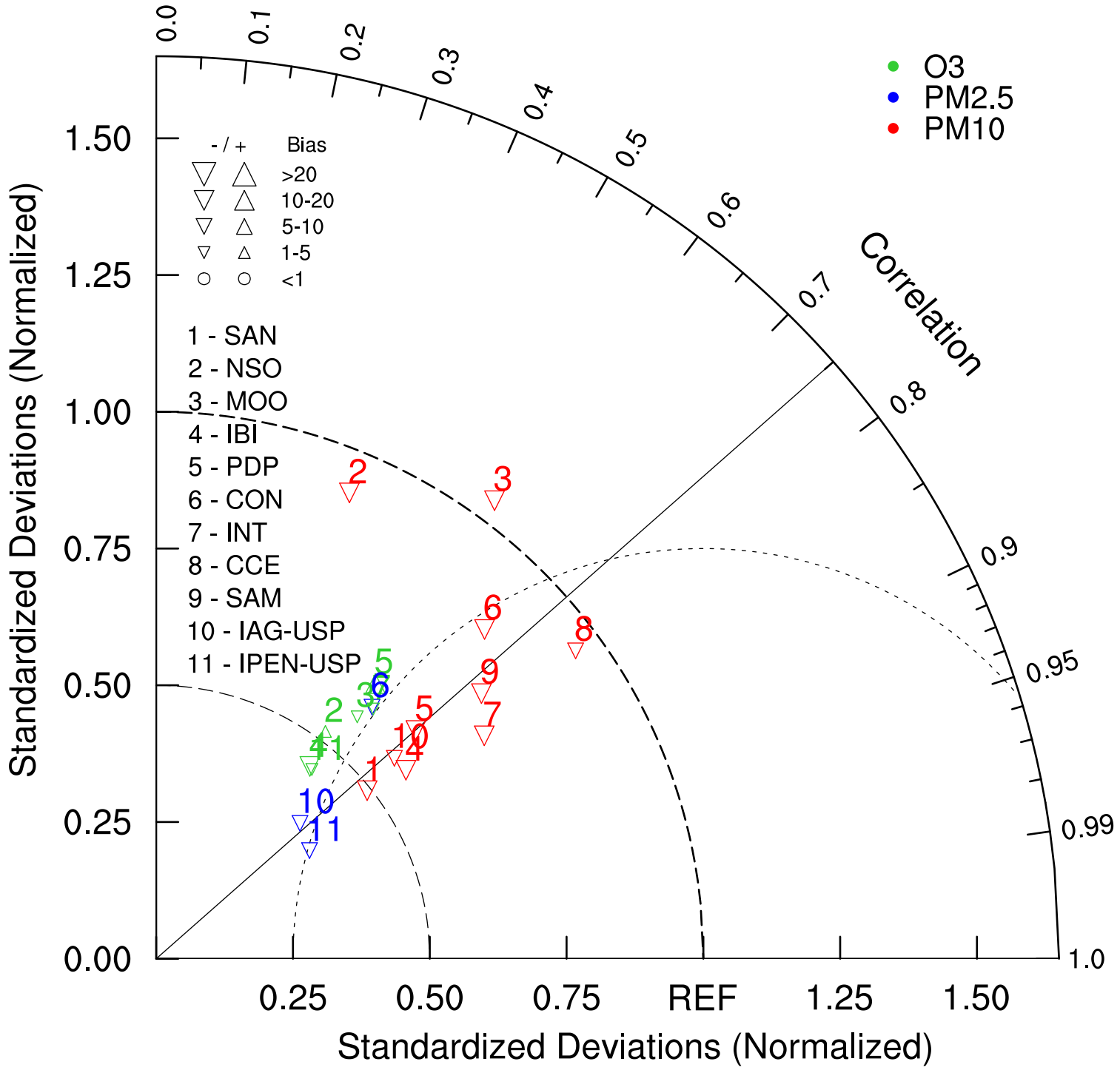
O3
PM2.5
PM10
- / + Bias
>20
10-20
5-10
1-5
<1
1 - SAN
2 - NSO
3 - MOO
4 - IBI
5 - PDP
6 - CON
7 - INT
8 - CCE
9 - SAM
10 - IAG-USP
11 - IPEN-USP
Correlation
0.0
0.1
0.2
0.3
0.4
0.5
0.6
0.7
0.8
0.9
0.95
0.99
1.0
Standardized Deviations (Normalized)
0.00
0.25
0.50
0.75
1.00
1.25
1.50
REF
Standardized Deviations (Normalized)

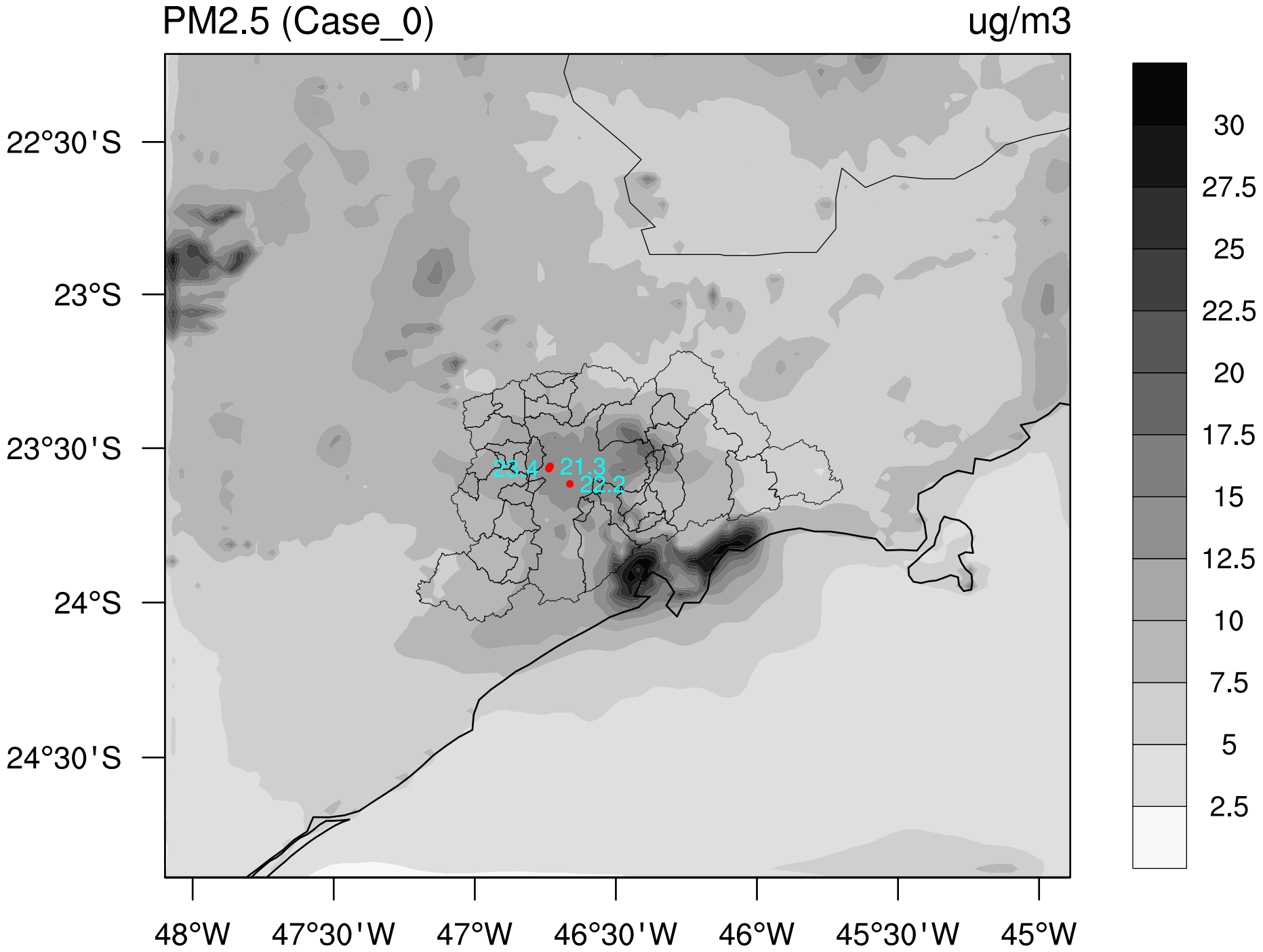
PM2.5 (Case_0)
ug/m3
22°30'S
23°S
23°30'S
24°S
24°30'S
48°W
47°30'W
47°W
46°30'W
46°W
45°30'W
45°W
23.4
21.3
22.2
30
27.5
25
22.5
20
17.5
15
12.5
10
7.5
5
2.5

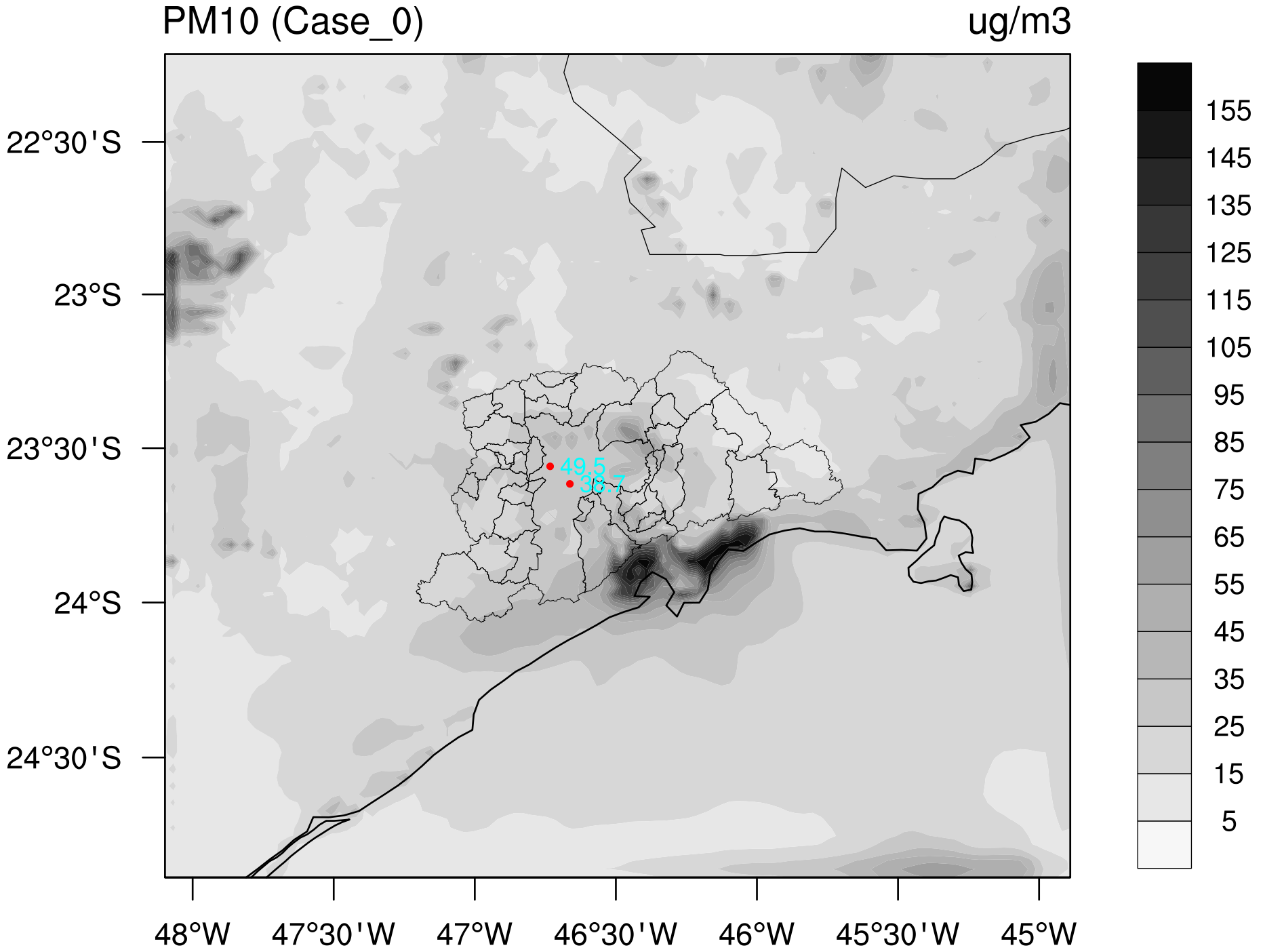
PM10 (Case_0)
ug/m3
22°30'S
23°S
23°30'S
24°S
24°30'S
48°W
47°30'W
47°W
46°30'W
46°W
45°30'W
45°W
49.5
38.7
155
145
135
125
115
105
95
85
75
65
55
45
35
25
15
5

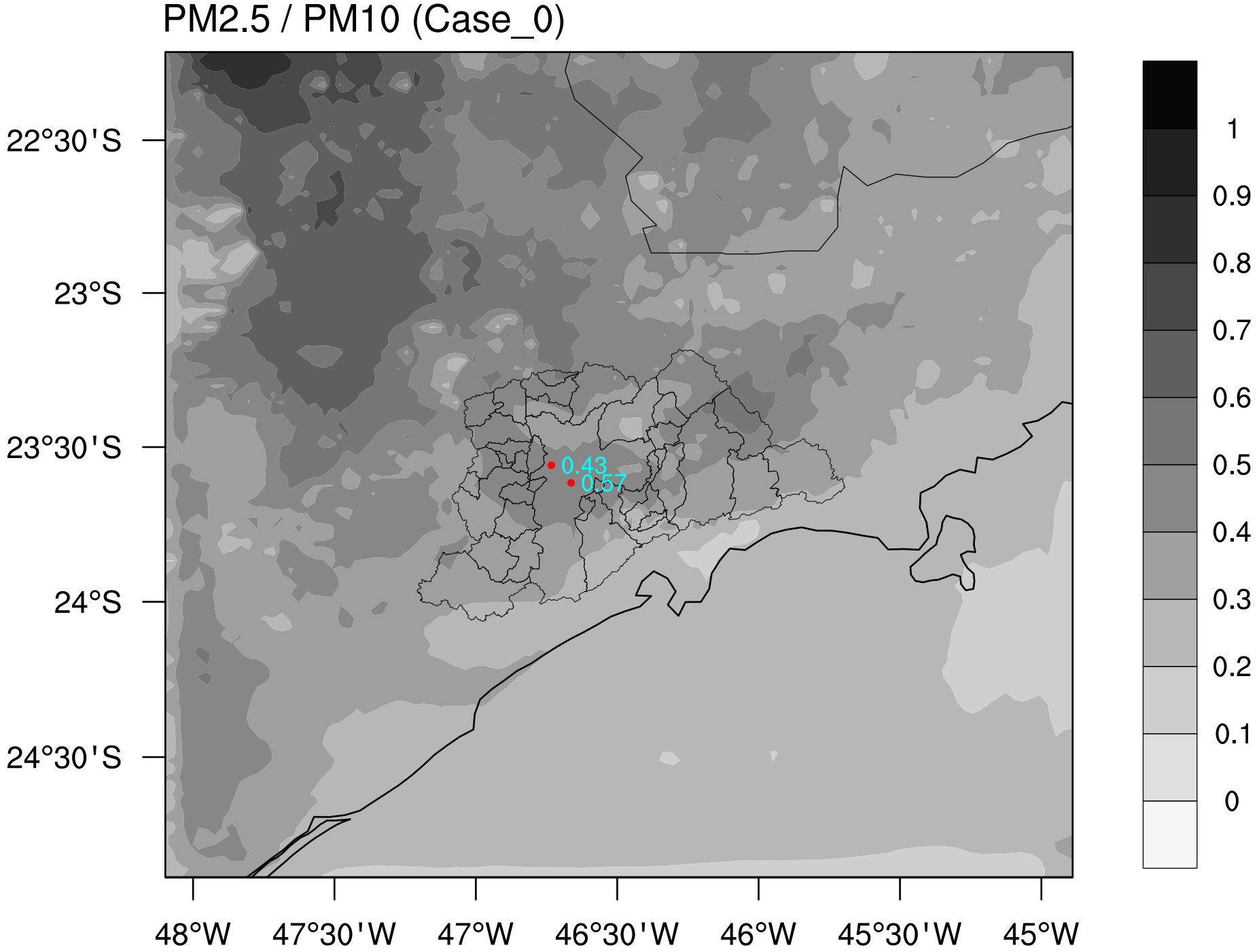
PM2.5 / PM10 (Case_0)
22°30'S
23°S
23°30'S
24°S
24°30'S
48°W
47°30'W
47°W
46°30'W
46°W
45°30'W
45°W
0.43
0.57
1
0.9
0.8
0.7
0.6
0.5
0.4
0.3
0.2
0.1
0

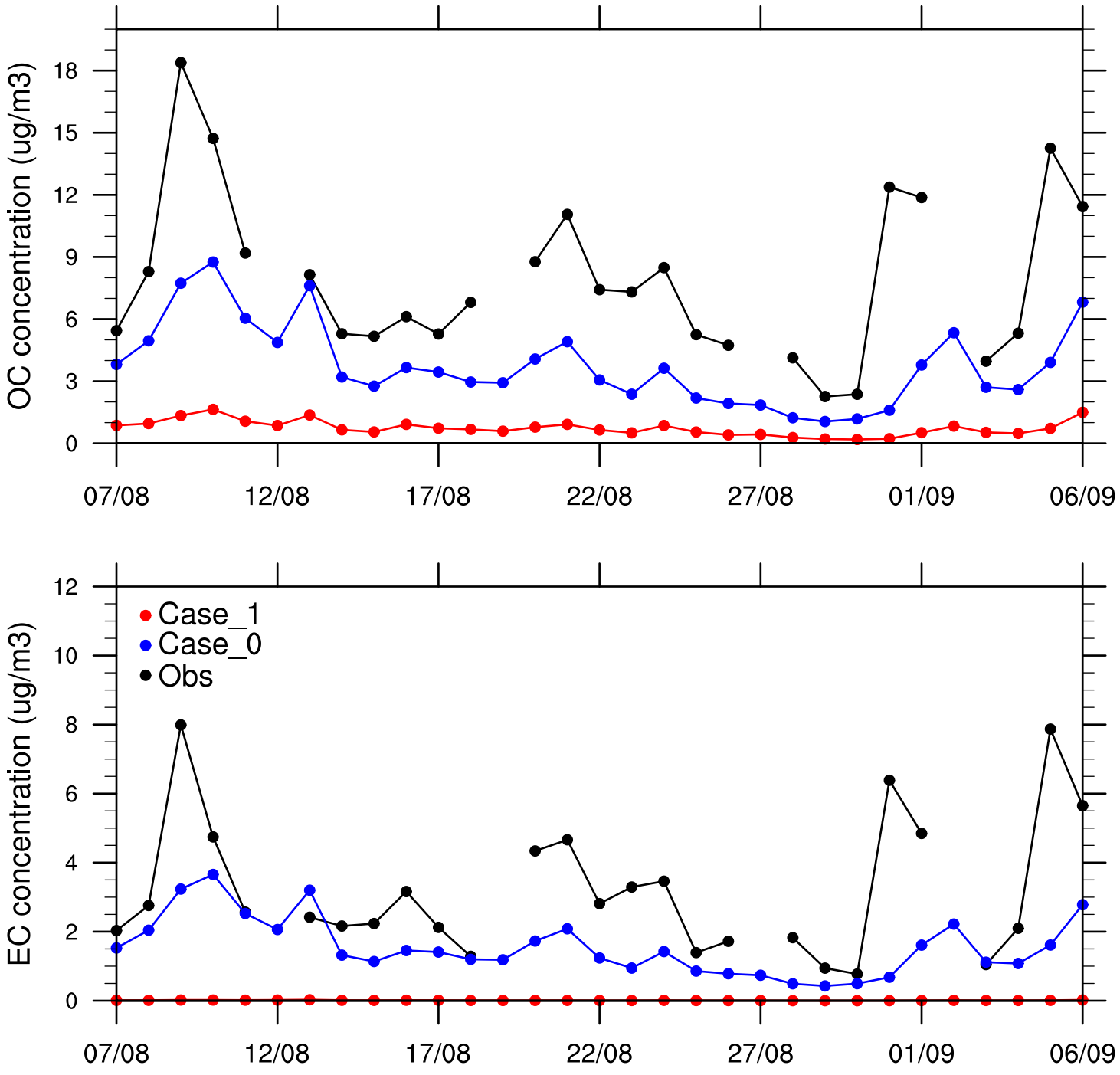
OC concentration (ug/m3)
18
15
12
9
6
3
0
07/08
12/08
17/08
22/08
27/08
01/09
06/09
EC concentration (ug/m3)
12
10
8
6
4
2
0
Case_1
Case_0
Obs
07/08
12/08
17/08
22/08
27/08
01/09
06/09

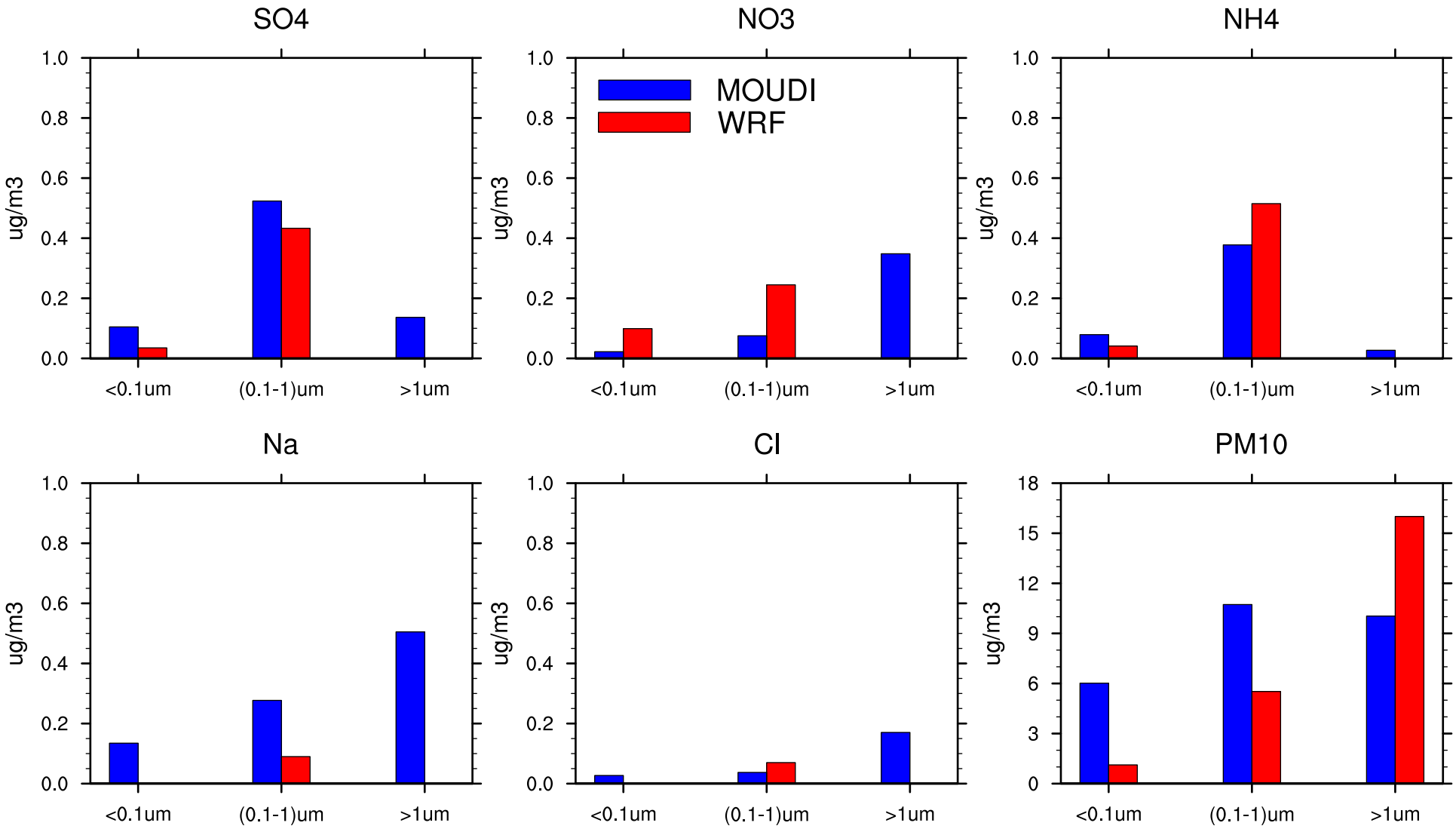
SO4
NO3
NH4
Na
Cl
PM10
MOUDI
WRF
ug/m3
<0.1um
(0.1-1)um
>1um
0.0
0.2
0.4
0.6
0.8
1.0
0
3
6
9
12
15
18

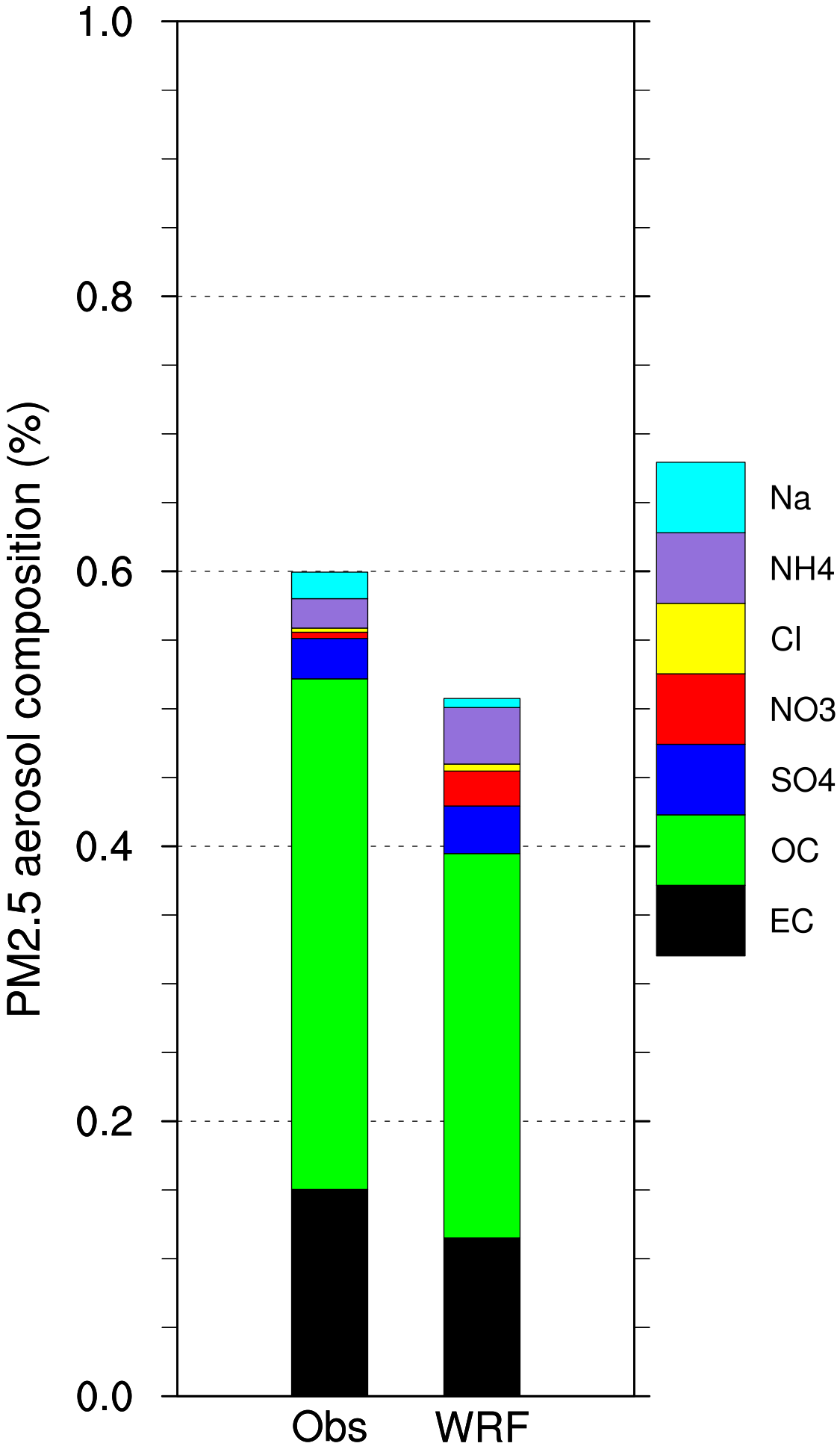
1.0
0.8
0.6
0.4
0.2
0.0
PM2.5 aerosol composition (%)
Obs
WRF
Na
NH4
Cl
NO3
SO4
OC
EC

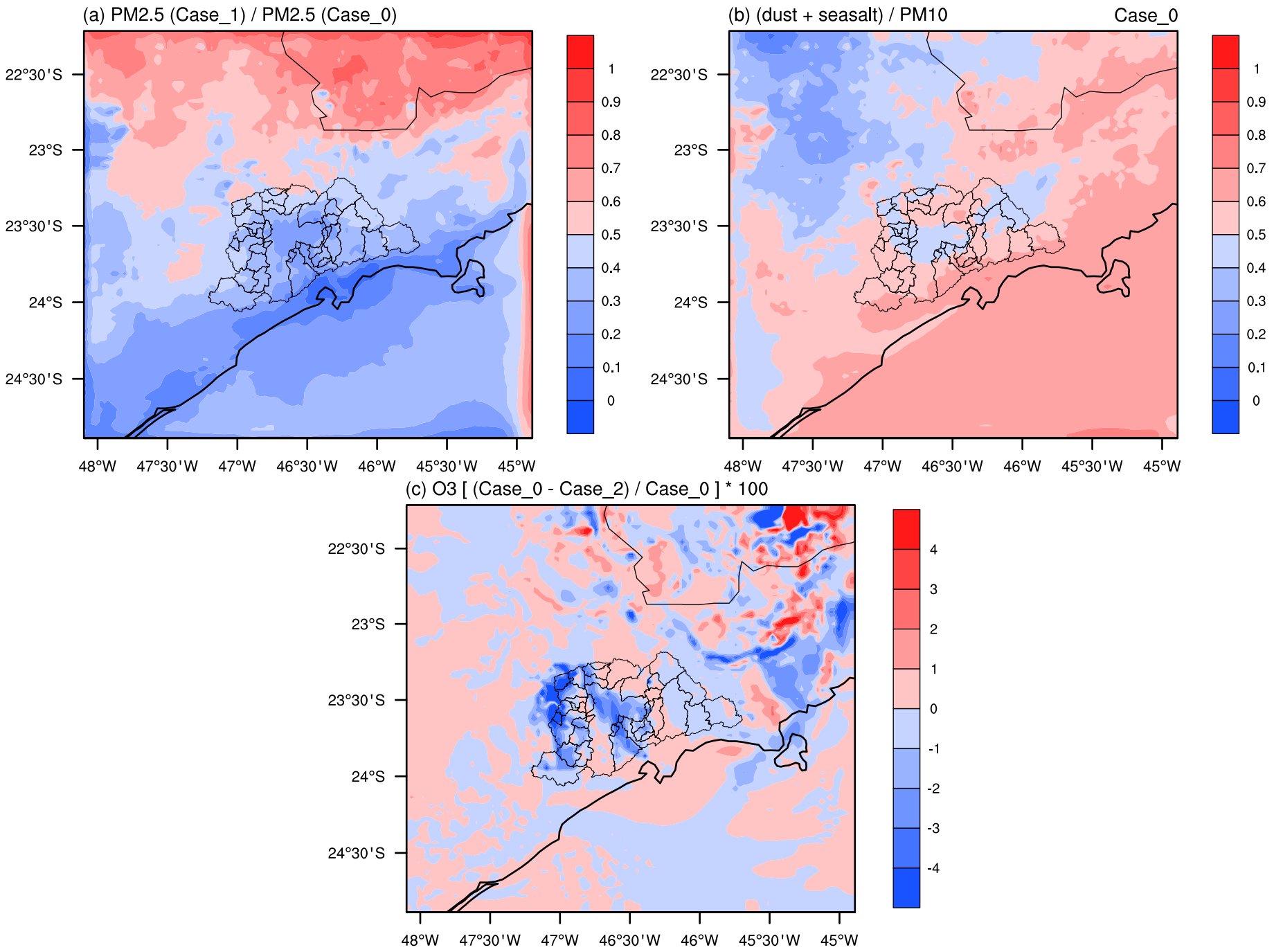
(a) PM2.5 (Case_1) / PM2.5 (Case_0)
(b) (dust + seasalt) / PM10
Case_0
(c) O3 [ (Case_0 - Case_2) / Case_0 ] * 100
22°30'S
23°S
23°30'S
24°S
24°30'S
48°W
47°30'W
47°W
46°30'W
46°W
45°30'W
45°W
1
0.9
0.8
0.7
0.6
0.5
0.4
0.3
0.2
0.1
0
4
3
2
1
0
-1
-2
-3
-4